1976

Detection of void fluctuations in reactor coolant channels by neutron noise analysis

Jerry Tong-Huei Lu
Iowa State University

Detection of void fluctuations in reactor coolant channels by neutron noise analysis

by

Jerry Tong-Huei Lu

A Dissertation Submitted to the
Graduate Faculty in Partial Fulfillment of
The Requirements for the Degree of
DOCTOR OF PHILOSOPHY

Department: Chemical Engineering and Nuclear Engineering
Major: Nuclear Engineering

Approved:

Signature was redacted for privacy.

In Charge of Major Work

Signature was redacted for privacy.

For the Major Department

Signature was redacted for privacy.

For the Graduate College

Iowa State University
Ames, Iowa

1976

TABLE OF CONTENTS

I. INTRODUCTION

The vapor (or "void") fraction, which represents the time-averaged volumetric fraction of vapor in a two-phase mixture, is one of the most important variables used to characterize the liquid-vapor flows that result from boiling in a water-cooled nuclear reactor. In a boiling water reactor (BWR), the presence of steam voids plays a direct role in the reactor, affecting such things as the pressure drop, neutron moderation, and the reactor power. The stochastic fluctuations of steam voids in the reactor coolant also have major dynamic effects on void fractions [1] as well as on noise sources in the reactors [2,3].

The application of noise analysis techniques to reactors is well recognized by many authors [2,4,5,6,7,8]. A number of fluctuating characteristics, including coolant flow rate [9,10], temperature [11,12], fuel element motion [13], and reactor power [6,14] have been investigated using noise techniques. With the use of in-core neutron detectors to monitor fluctuations in reactors in recent years [15,16], reactor noise research is being directed toward obtaining a better understanding of the noise signals in power reactors.

In the case of the boiling water reactor, in-core neutron noise has been described in terms of the detector response to "local" and "global" driving sources [15,17,18,19]. The local driving source, which is a direct neutron noise attributed to steam voids, has been used to obtain information on the vapor velocity in the coolant channel [15]. The fluctuation of steam voids also causes indirect fluctuations in the neutron density. These arise from reactivity changes due to fluctuations in flow rate, cool-

ant density, and pressure [3,20]. The latter effects are included in the global driving source. This source is rather well understood due to the work of the number of authors. In the case of the local source, the theoretical and experimental basis does not seem to be as completely developed.

It is the purpose of this work to obtain a more detailed understanding of the local driving source due to coolant voids in a boiling water reactor coolant channel. The study has been initiated to investigate the characteristics of the neutron field and detector response perturbations due to the random nature of coolant void formation and motion in a water channel.

An out-of-core test assembly, which utilizes air and steam voids, has been used to study the effect of voids on the transmission of thermal-neutrons through water. The test assembly consists of a vertical open aluminum water channel positioned near a fission chamber. Voids were produced by an air bubble generator and an electric heater. The thermalized neutron flux from the thermal column of the Ames Laboratory Research Reactor was used as the radiation source. The stochastic component of the transmitted neutron beam has been analyzed in terms of auto-power spectral densities and probability density functions.

The experimental investigation has been concerned with the following aspects of coolant voids in the test assembly: (1) a comparison of air-water and steam-water mixtures, (2) the effect of the bubble size and generation rate, (3) the space dependence along the channel, and (4) the detection of the two-phase flow regime in the channel.

In order to have an independent comparison with the neutron detector results, measurements were also made using a plexiglas tank which contained a photocell and light source. The plexiglas tank was also utilized to pro-

vide a visual confirmation of the void motion for the air-void experiment. Photographs of the bubble motion and time-history records of noise signals were also obtained to give additional comparisons with the frequency and time domain results.

II. LITERATURE REVIEW

The historical development of nuetron noise analysis has been reviewed by Seifritz and Stegemann [21], Kosaly [8], and Saito [7] in recent years. These review papers give a clear picture of the state of the art of noise analysis in nuclear reactors. Since the primary objective of this investigation was to study the void fluctuations in a reactor coolant channel using neutron noise analysis, the literature survey is primarily directed to work performed by other investigators on two-phase flow in a reactor coolant channel and the use of noise techniques for the detection of boiling in nuclear reactor.

A. Two-Phase Flow and Void Fraction in Reactor Coolant Channels

The importance of two-phase flow is discussed in many references. The suspension of discrete bubbles (or voids) in a continuous liquid is an essential characteristic in a liquid-cooled reactor in which boiling is taking place. The bubbles begin to form on the heated surface when the wall temperature reaches a certain value and then break away from the surface. The different regimes of boiling are shown in Fig. 1 [22]. For the boiling water reactor, the coolant is operating in the bubble region, i.e. in Regions II and III. The region where the temperature increases beyond the critical heat flux (point a in Fig. 1) is avoided.

The process of bubble growth is complex, and there is considerable controversy as to exactly how bubbles are initially formed on the heat-transfer surface [23]. Excellent summaries of the status of knowledge of

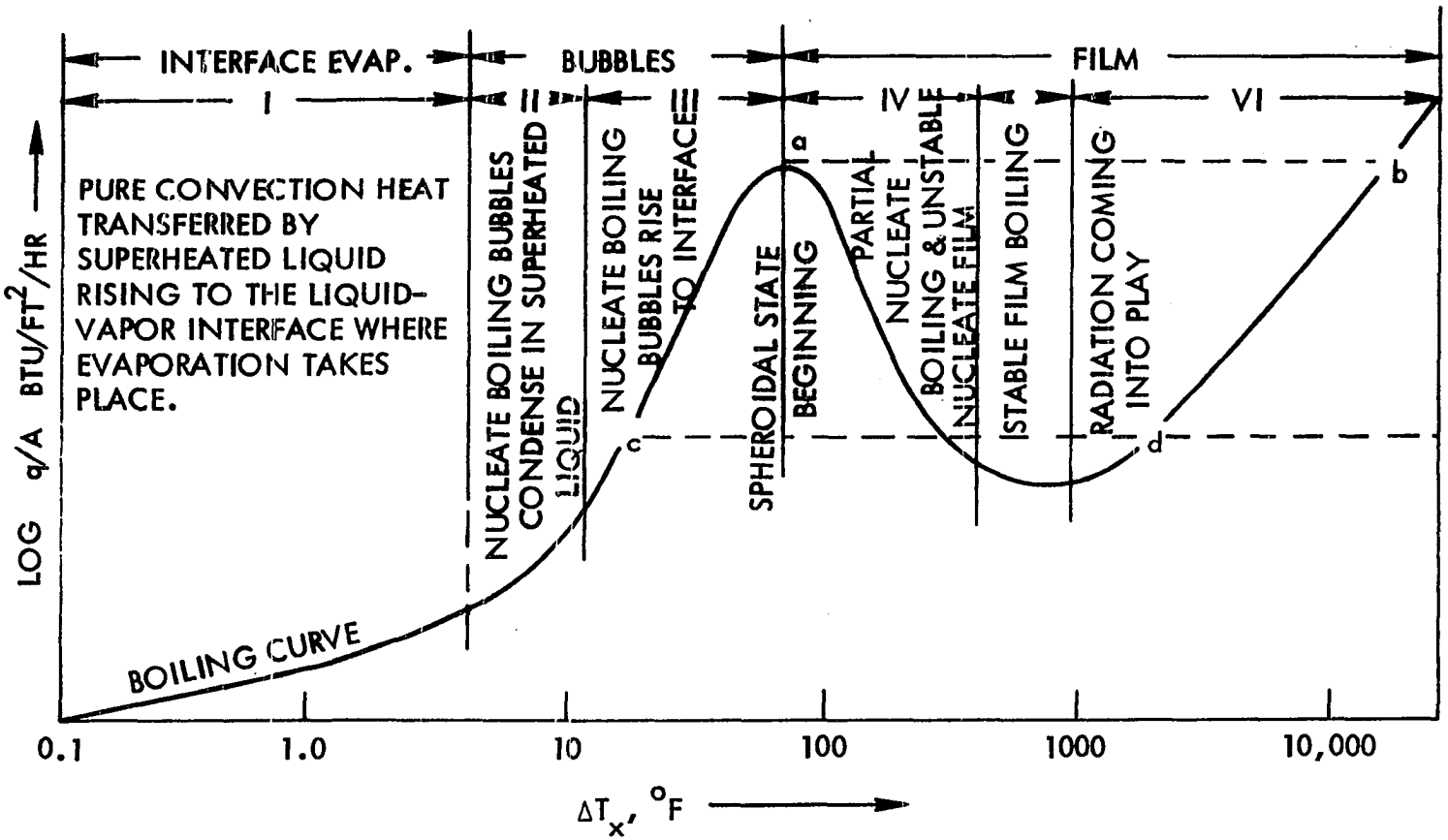

Fig. 1. Characteristic boiling curve [22]

boiling heat transfer have been reviewed by Rehsenow [22], Leppert and Pitts [24], Tong [25], and Wallis [26].

When discussing two-phase flow phenomena, it is appropriate to discuss flow regime configurations and analysis. However, it is generally quite difficult to be able to specify with any degree of accuracy when a given flow regime exists and where transitions occur [27]. For normal operation of a BWR, the basic flow regime patterns are shown schematically in Fig. 2. In a diabatic system, these flow regimes occur sequentially along the heated surface from the inlet to the exit in a once-through evaporator. Fig. 3 shows a diagram of the development of flow regimes in diabatic systems. The situation in a BWR rod bundle is best represented by displays such as shown in display G of Fig. 3.

Little is now known about the exact type of two-phase flow taking place in reactor systems [27,28]. It is conceivable to determine the mechanism of two-phase flow by predicting the void fraction in the reactor coolant channel. To predict the vapor formation and profiles in the coolant channel, Houghton [29,30] treated the bubble as a free particle and used Brownian motion to describe the bubble movement in a liquid. Levy [31] applied a bubble force balance from the heated surface to calculate the void fraction. A generalized void fraction model was proposed by Sha [32]. In his model, the steam bubbles were also considered to be free particles, and the continuity equation was applied to solve for the radial and axial distribution of void fractions in the channel. Techy and Szabados [33] considered the random motion of steam bubbles and took the probability distribution of bubble velocities into account. The diffusion approach

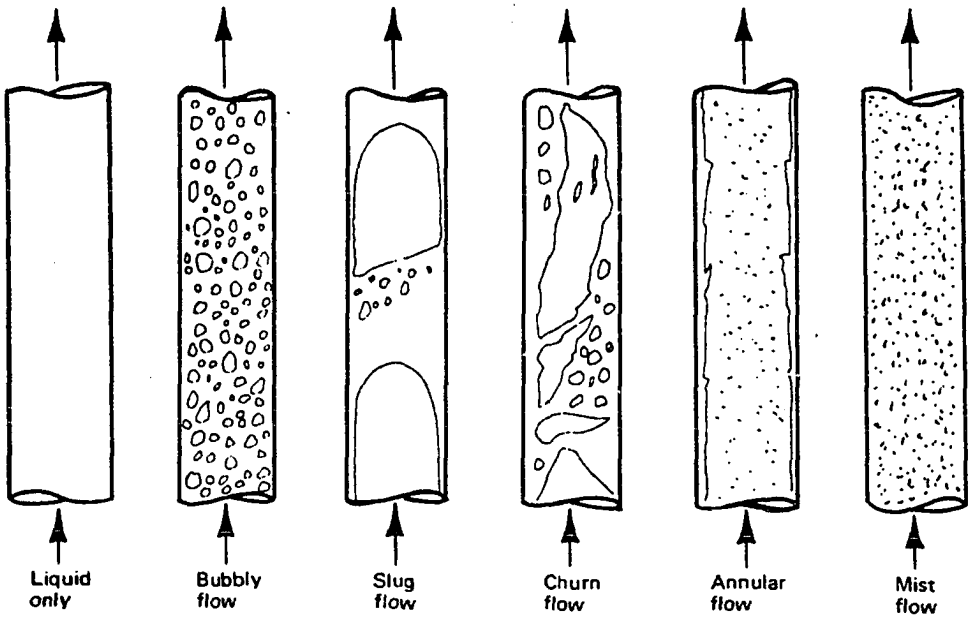

Fig. 2. Typical flow regime patterns in vertical flow [27]

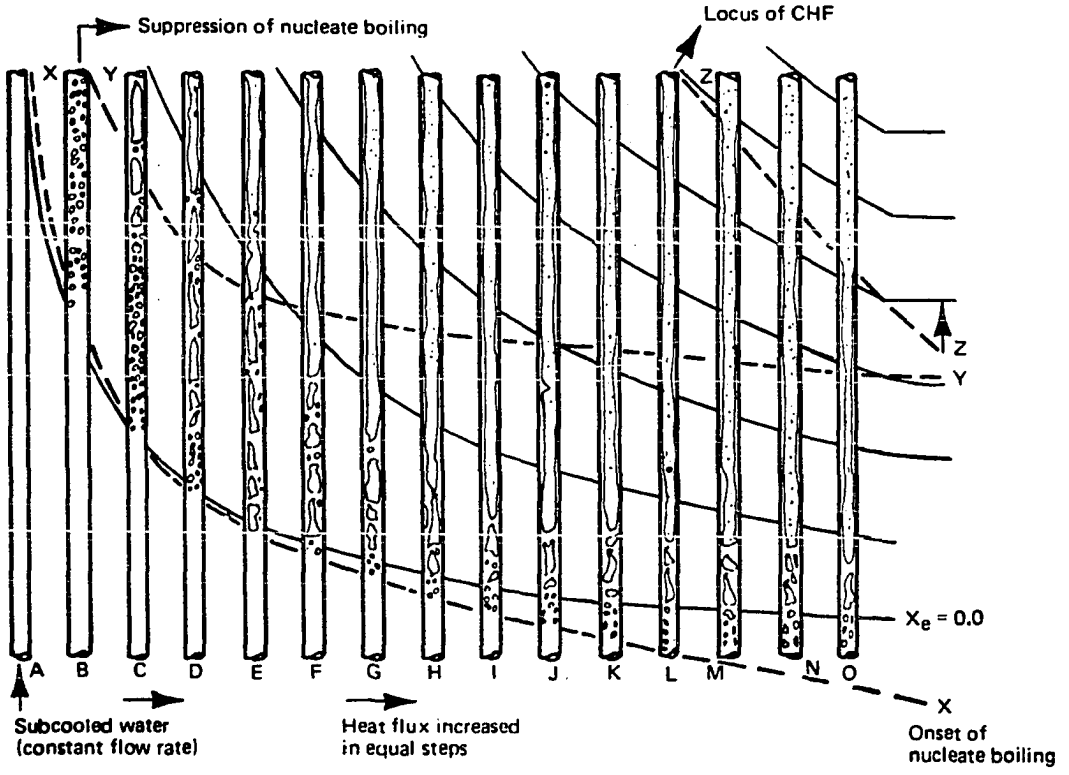

Fig. 3. Diabatic Flow Regimes [27]

formulated by Houghton [29] and Sha [32] can be proved by this theoretical basis of bubble motion.

All theoretical models in the references are used to predict the average void fractions in the reactor coolant channel. The fluctuations of bubbles both in space and time have not been included.

B. Detection Methods for Boiling in Nuclear Reactors

The detection of the onset of boiling in nuclear reactors is of importance because many reactors, such as BWR's, are required to operate at as high a power as possible to obtain maximum efficiency and to avoid reaching the critical heat flux. However, the energetic environment in nuclear reactors gives considerable restriction on the type of equipment that can be operated and even rules out the use of some methods of detection, for example, the optical technique. Saxe [2] compared two detection techniques, one based on neutron flux measurements and the other is based on acoustic measurements. It was suggested, in principle, that the acoustic method for the detection of boiling in reactors is more direct, because two or possibly three frequency ranges are available. Later in two papers Saxe [34] and Saxe et al. [35] again compared possible methods to detect boiling. The ultrasonic and acoustic methods were suggested as best for incipient boiling detection in nuclear reactors. However, the existence of the high frequency spectrum from cavitation noise makes the detection of boiling by these two methods doubtful in many cases [36].

Bonnet and Osborn [37] proposed a method utilizing a gamma ray technique to determine the initiation of bulk boiling in a sodium-cooled fast reactor as well as in a boiling water reactor. This technique consisted of

introducing a standing acoustic wave in a coolant channel of the core. A ratio of gamma rays monitored with and without the acoustic waves was strongly coupled to the acoustic velocity which is sensitive to the void fraction in the channel. A drastic reduction in the acoustic velocity was found with the formation of voids.

As far as reactor monitoring techniques are concerned, the choice of which method to use in a given case is often determined by considerations of convenience and feasibility [37]. With the application of self-powered in-core detectors [15,16], neutron fluctuation measurements seem to be more feasible and economic for boiling detection in a reactor coolant channel.

C. Experimental Investigations of Void Fluctuations in the Reactor Coolant Channel

The earliest investigation of boiling fluctuations and measurements in the reactor was carried out by Boyd [38] in 1959. A neutron-sensitive ion chamber was used to detect nucleate boiling. Voids in the water moderator, caused by boiling, decrease the moderation and cause fluctuations in the thermal neutrons. De Shong [39] studied the reactor flux noise and found a resonance peak in the energy-frequency spectrum. He suggested that "boiling noise" is due to the random variation of the steam generation rate.

Colomb and Binford [40] put a heater inside an Oak Ridge National Laboratory reactor core. A power spectral density was measured and compared with that without the heater. This was suggested as a possible method to detect when boiling occurs. Thie [41] referred to the interaction of voids and neutron flux moderation as "thermalization noise" and identified this noise source from in-core neutron detectors at the Pathfinder Atomic Power Plant [42]. An experimental analysis of the inherent fluctuations (noise)

in a nuclear power reactor was conducted by Rajagopal [14]. A resonance peak related to nucleate boiling was found, and the nature of the dependence of the resonance on reactor power suggested that a relation existed between nucleate boiling and the resonance.

The most comprehensive experimental work relating to neutron noise in power reactor has been done by Seifritz [16] and Stegemann et al. [15] at the Lingen Boiling Water Reactor (KWL). A movable prompt responding self-powered cobalt incore detector positioned in a dry thimble was used to detect the neutron fluctuations in numerous axial positions. The experimental results showed the space dependence of neutron flux fluctuations along the coolant channel as well as the characteristics of boiling zones in the reactor.

A rather complete summary of noise analysis experiments conducted in BWR's is listed in Ref. 16, and it can be used to obtain information on previous work relating to neutron fluctuations in nuclear reactors.

D. Void Noise Models in Nuclear Reactors

The "boiling noise," which stands as a major noise source in BWR's, was established by De Shong [39] in 1959. However, due to the complexity of the phenomenon in the BWR, theoretical studies of void noise were quite limited in the early 1960's. In 1968 Nomura [3] developed a reactor model which included the noise source due to voids generated at steady state heat output. The time series of random void generation along a boiling channel was assumed to be independent of frequency. The model neglects the direct (or local) neutron fluctuation effects on a detector due to void generation but includes fluctuations in flow velocity, pressure, and fuel temperature due to the boiling noise. These fluctuations result in reactivity varia-

tions and in turn neutron flux. The result of the study was compared with an experiment on the Japan Power Demonstration Reactor and gave a promising similarity.

In analyzing reactor noise from the coolant, Mogil'ner [20] treated the neutron noise as induced from two parts: the "inherent noise" of gas bubbles and pressure fluctuations. In this model, the inherent noise is induced by the shot-noise of the bubbles entering the system. The presence of gas bubbles leads to the existence of pressure fluctuations and then to additional fluctuations of reactivity. By comparing his model to experiments, Mogil'ner was able to deduce the void fraction and the average volume of a bubble.

In all of the models considered in these references, it was assumed that void fluctuations are fed back to reactivity and finally to neutron fluctuations. Rothman [17], however, presented a method, restricted to the higher frequency ranges, where the feedback effects are neglected. Based on the assumption of a Poisson distribution of the local voidage in the coolant channel and the use of the collison probability approach, he presented an analysis of the detector response arising from random local aggregations of bubbles in the reactor channel.

Wach and Kosaly [18] investigated one of the experiments performed in a BWR and proposed a model which included the joint effect of local and global noise sources on in-core neutron detectors. The results of the model predicts the frequencies of resonance peaks in the gains of the transfer function obtained from the experimental results. Although this model is a rather phenomenological one, it strongly supports the thesis

that the local driving noise sources (e.g. void fluctuations) play an important role in the in-core noise measurements.

It is clear from the literature review that neutron noise fluctuations due to void generation in the reactor coolant channel can be used to provide information on the operation of at-power nuclear reactors. It is necessary to have a complete understanding of the characteristics of void generation in the coolant channel both in experimental and theoretical work. This will aid in the interpretation of observed neutron noise results and facilitate relating them to reactor parameters during normal or even abnormal reactor operation.

III. ANALYSIS OF VOID FLUCTUATIONS BY NEUTRON NOISE TECHNIQUES

A. Response of the Nuetron Detector to Voids

The neutron attenuation (or transmission) measurement, which consists of a neutron detector and a reactor neutron source, has been shown to be a feasible diagnostic tool for time-averaged void fraction measurements [43, 44,45]. However, the effect of void fluctuations in the coolant channel limits the applications of this technique in practice [1].

Consider a narrow, collimated, monoenergetic and time-independent neutron beam which is projected perpendicular to a planar coolant channel of liquid containing upward-moving voids as shown in Fig. 4. The void fraction at time t is defined by

$$\alpha(z,t) = \frac{\sum_i \Delta X_i(z,t)}{X_o} \tag{3.1}$$

where Xo is the thickness of the coolant channel.

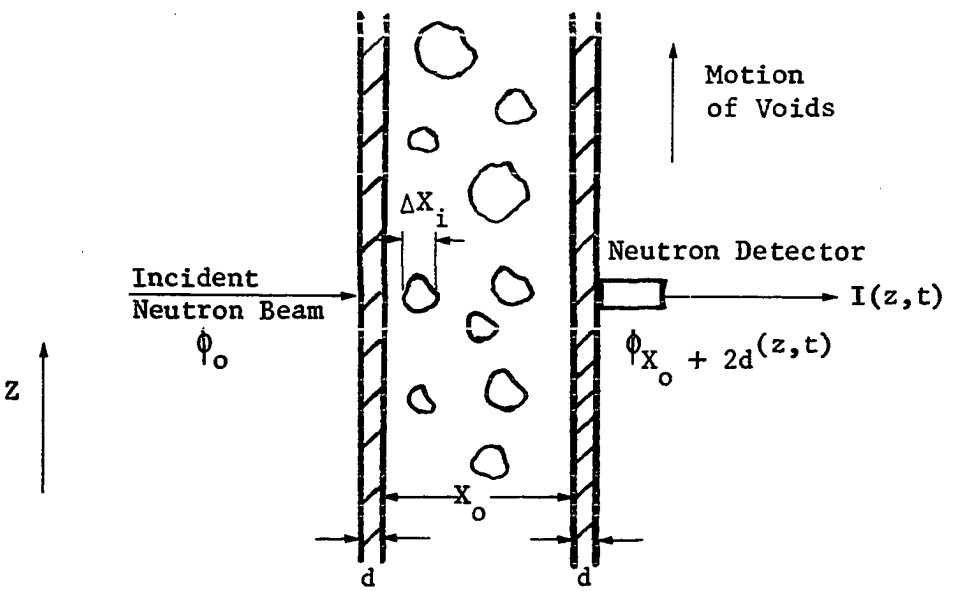

Fig. 4. Schematic representation of voided liquid flow channel

The emerging neutron beam can be expressed in terms of the incident beam as

$$\phi_{X_o+2d}(z,t) = \phi_o \exp(-\mu_p 2d) \exp\left\{-\mu_o X_o [1-\alpha(z,t)]\right\} \tag{3.2}$$

where μ_p and μ_o are defined as the linear attenuation parameters for the channel wall and the liquid medium, respectively.

The current, I(z,t), of the neutron detector is given by

$$I(z,t) = G e_d \phi_{X_o+2d}(z,t) \tag{3.3}$$

where e_d is the detector efficiency and G is the geometry factor of the detector. Substituting Eq. (3.2) into Eq. (3.3) yields

$$I(z,t) = G e_d \phi_o \exp(-\mu_p 2d) \exp\left\{-\mu_o X_o [1-\alpha(z,t)]\right\}. \tag{3.4}$$

In case of a static void fraction in the channel, i.e. $\alpha(z,t) = \bar{\alpha}$ = constant, Eq. (3.4) can be expressed as

$$\overline{I(z,t)} = G e_d \phi_o \exp(-\mu_p 2d) \exp[-\mu_o X_o (1-\bar{\alpha})]. \tag{3.5}$$

When there are no voids in the coolant channel, Eq. (3.5) is further expressed as

$$I_o = G e_d \phi_o \exp(-\mu_p 2d) \exp(-\mu_o X_o). \tag{3.6}$$

Eq. (3.5) and (3.6) have been applied to average void fraction measurements [43,44,45].

For the fluctuating voids in a coolant channel, the stochastic characteristic of coolant voids can be observed by the neutron detector. Assume linear approximations of detector response and void fractions, and express I(z,t) and $\alpha(z,t)$ as

$$I(z,t) = \overline{I(z,t)} + i(z,t) \tag{3.7}$$

and

$$\alpha(z,t) = \bar{\alpha} + \alpha'(z,t) \tag{3.8}$$

where $i(z,t)$ and $\alpha'(z,t)$ are fluctuating components of $I(z,t)$ and $\alpha(z,t)$, respectively. Substituting Eqs. (3.7) and (3.8) into Eq. (3.5) results in

$$i(z,t) = \overline{I(z,t)} \cdot \left\{ \exp[\lambda\alpha'(z,t)] - 1 \right\} \tag{3.9}$$

where λ is equal to $\mu_o X_o$.

Eq. (3.9) gives a direct expression for the response of the neutron detector to the void fluctuation in the coolant channel. If $|\lambda\alpha'(z,t)| \ll 1$, a linear approximation of the exponential function can be made, and Eq. (3.9) becomes

$$i(z,t) \cong \overline{I(z,t)} \cdot [1 + \lambda\alpha'(z,t) - 1] = \overline{I(z,t)} \cdot \lambda\alpha'(z,t). \tag{3.10}$$

For a fixed thickness of the coolant channel, a linear relationship between the fluctuating current and void fraction results when $|\lambda\alpha'(z,t)|$ is very much less than one.

A sensitive response of the neutron detector to the fluctuations of voids in the coolant channel is indicated by Eq. (3.9). However, due to the unknown function $\alpha'(z,t)$, the fluctuating current, $i(z,t)$ is in an implicit expression.

In deriving Eq. (3.9), it is assumed that ϕ_o is time-independent. However, the neutron fluctuation due to the branching and power noise exists in practical cases. In case the neutron flux passes through a thermal column, as in this study, the branching and power noise can be considered as a "white" noise, which means that the power spectrum is uniform over all frequencies. The instrumentation noise, which is also "white," can be included in the branching and power noise and termed as background noise. Adding the background noise source to the fluctuation response of

the neutron detector, the total fluctuating current from the neutron detector can be expressed as

$$i_T(z,t) = i_v(z,t) + i_b(z,t) \tag{3.11}$$

where $i_T(z,t)$ is the total fluctuating current of the neutron detector, $i_v(z,t)$ is the corresponding fluctuation current due to voids as given in Eq. (3.9), and $i_b(z,t)$ is the fluctuating current of background noise sources including the branching and power noise and the instrumentation noise. In case of large fluctuations of coolant voids, $i_v(z,t)$ is greater than $i_b(z,t)$, and the total fluctuation, $i_T(z,t)$, can be well represented by the void fluctuations and is given by

$$i_T(z,t) \cong i_v(z,t). \tag{3.12}$$

B. Analysis of Void Fluctuations in the Time Domain by the Probability Density Function

The probability density function (PDF) of random data describes the probability that data will assume a value within some defined range at any instant of time [46]. The PDF furnishes information concerning the properties of the data in the amplitude domain. Consider the sample time history record of the fluctuating current $i_T(z,t)$. The probability density function for the signal $i_T(z,t)$ is defined as

$$p[i_T(z)] = \lim_{\Delta i_T \to 0} \frac{\text{Prob}[i_T(z) \leq i_T(z,t) \leq i_T(z) + \Delta i_T]}{\Delta i_T} \tag{3.13}$$

where Δi_T is the window between i_T and $i_T + \Delta i_T$.

To determine the PDF of the fluctuating current due to voids, the sample time record of $i_v(z,t)$ has to be isolated from that of the background noise source, $i_b(z,t)$. However, in the case of fluctuating voids, as

expressed by Eq. (3.12), the PDF of void fluctuations, $i_v(z,t)$ is approximately equal to the total current fluctuations, $i_T(z,t)$. The probability density functions of the background noise sources can be calculated from the sample time record of $i_b(z,t)$, which is recorded from the neutron detector without voids in the coolant channel.

C. Analysis of Void Fluctuations in the Frequency Domain by the Auto-Power Spectral Density Function

The auto-power spectral density function (also called the power spectral density) of random data describes the general frequency composition of the data in terms of the spectral density of its mean square value [46]. It bears important relationships to the basic characteristics of the physical system involved. Historically, the auto-power spectral density (APSD) is calculated from the Fourier transform of the autocorrelation function of the random data. For a sample time history of a stationary record X(t) over the observation time T, the autocorrelation function is defined as

$$R_x(\tau) = \lim_{T\to\infty} \frac{1}{T} \int_0^T X(t)X(t+\tau)dt \tag{3.14}$$

where τ is the time displacement between time t and $t+\tau$.

For stationary random data, the power spectral density function $S_x(f)$ is the Fourier transform of $R_x(t)$, i.e.

$$S_x(f) = \int_{-\infty}^{\infty} R_x(t) e^{-j2\pi ft} dt. \tag{3.15}$$

If the fluctuating current of the neutron detector, $i_T(z,t)$ is composed of two parts as expressed in Eq. (3.11), i.e.

$$i_T(z,t) = i_v(z,t) + i_b(z,t), \tag{3.11}$$

then for the two stationary, uncorrelated random processes of $i_v(z,t)$ and $i_b(z,t)$, the autocorrelation function is given by

$$R_{iT}(z,\tau) = R_{iv}(z,\tau) + R_{ib}(z,\tau) \tag{3.16}$$

where

$$R_{iT}(z,\tau) = \lim_{T\to\infty} \frac{1}{T} \int_0^T i_T(z,t) i_T(z,t+\tau)\, dt \tag{3.17}$$

$$R_{iv}(z,\tau) = \lim_{T\to\infty} \frac{1}{T} \int_0^T i_v(z,t) i_v(z,t+\tau)\, dt \tag{3.18}$$

$$R_{ib}(z,\tau) = \lim_{T\to\infty} \frac{1}{T} \int_0^T i_b(z,t) i_b(z,t+\tau)\, dt. \tag{3.19}$$

Applying the Fourier transform, Eq. (3.16) becomes

$$S_{iT}(z,f) = S_{iv}(z,f) + S_{ib}(z,f) \tag{3.20}$$

where

$$S_{iT}(z,f) = \int_{-\infty}^{\infty} R_{iT}(z,\tau) e^{-j2\pi f\tau}\, d\tau \tag{3.21}$$

$$S_{iv}(z,f) = \int_{-\infty}^{\infty} R_{iv}(z,\tau) e^{-j2\pi f\tau}\, d\tau \tag{3.22}$$

$$S_{ib}(z,f) = \int_{-\infty}^{\infty} R_{ib}(z,\tau) e^{-j2\pi f\tau}\, d\tau\ . \tag{3.23}$$

For a finite observation time T, in practice, the power spectral density function can be calculated directly from the sample time record without calculating the autocorrelation function. This is derived by substituting Eqs. (3.17), (3.18), (3.19) into Eqs. (3.21), (3.22), and (3.23). The following equations are obtained:

$$S_{iT}(z,f) = \frac{2}{T}.I_T^*(z,f).I_T(z,f) \tag{3.24}$$

$$S_{iv}(z,f) = \frac{2}{T}.I_v^*(z,f).I_v(z,f) \tag{3.25}$$

$$S_{ib}(z,f) = \frac{2}{T}.I_b^*(z,f).I_b(z,f) \tag{3.26}$$

where

$$I_T(z,f) = \int_0^T i_T(z,t)e^{-j2\pi ft}dt \tag{3.27}$$

$$I_v(z,f) = \int_0^T i_v(z,t)e^{-j2\pi ft}dt \tag{3.28}$$

$$I_b(z,f) = \int_0^T i_b(z,t)e^{-j2\pi ft}dt. \tag{3.29}$$

$I_T^*(z,f)$, $I_v^*(z,f)$, and $I_b^*(z,f)$ are complex conjugates of $I_T(z,f)$, $I_v(z,f)$, and $I_b(z,f)$, respectively. To calculate the Fourier transform in Eqs. (3.27), (3.28), and (3.29), a fast Fourier transform (FFT) algorithm [47] is available for computer application. It should be noted that the APSD calculations from Eqs. (3.24), (3.25), and (3.26) are raw power spectral densities. The averaging process should be applied to obtain better results.

The void fluctuation, $\alpha'(z,t)$, in the coolant channel, as expressed in Eq. (3.9) is a very complicated function as far as voids in the two-phase flow. As shown by many investigators, for example, Refs. 48, 49, 50, 51, many parameters are responsible for void fluctuations. The void fluctuation in boiling flow is susceptible to thermal-hydrodynamic instabilities and may cause flow oscillations [52,53,54]. Nevertheless, there is not an adequate description of the phenomena of void fluctuations in a coolant

channel available. It is the purpose of this study to obtain a better understanding, from an experimental investigation, of the void fluctuation in the reactor coolant channel. The power spectral density measurement is a useful technique to determine the characteristics of the physical system as given in Eq. (3.20) when $\alpha'(z,t)$ is an unknown function of time. For an out-of-core experiment with a thermalized neutron flux, the APSD of the background noise $S_{ib}(z,f)$ in Eq. (3.20), is approximately "white." This implies that a constant APSD in the frequency domain can be assumed and expressed as

$$S_{ib}(z,f) = A. \tag{3.30}$$

Substituting Eq. (3.30) into Eq. (3.20), the APSD of the detector response then becomes

$$S_{iT}(z,f) = S_{iv}(z,f) + A \tag{3.31}$$

or

$$S_{iv}(z,f) = S_{iT}(z,f) - A. \tag{3.32}$$

The APSD of void fluctuations in the coolant channel is thus determined from Eq. (3.32). The APSD of the detector fluctuating noise, $S_{iT}(z,f)$ and the constant A are calculated from measurements with and without voids in the coolant channel. For the fluctuating voids in the coolant channel, $S_{iv}(z,f)$ is usually several orders higher in magnitude than that of the background noise. The APSD can then be expressed as

$$S_{iT}(z,f) \cong S_{iv}(z,f). \tag{3.33}$$

In this study, the fluctuating noise signals were taken from the output of a picoammeter. The output polarity, for the instrument used in this experiment, is opposite of the input signal polarity. Hence, in terms of

voltage output, a negative sign should be added to Eq. (3.9) to be consistent with the experimental results.

IV. EXPERIMENTAL APPARATUS

A. Test Section

Experimental measurements were carried out for two types of voids: (1) air voids and (2) steam voids. The open water aluminum channel shown both in Fig. 5 (a) and (b) was used as a coolant channel. It was approximately 37 inches long and 3¼ in. x 3/4 in. in cross-section. The thickness of the channel was selected so that the intensity of the transmitted neutron flux was adequate for statistical response considerations. A thin steel channel supporter was built to make the coolant channel steady when air or steam voids were supplied. It was also used to keep the vibration of the channel from affecting the detector. A string connected to the channel and mounted on a pulley was used to move the coolant channel up and down relative to the neutron beam for the space-dependent measurement of voids.

Fig. 5(a) shows the test section assembly with air voids. A 3/16 in. I.D. stainless steel tube was used as a bubble generator. One or more small holes were drilled to serve as an orifice for the generation of air voids. Different hole sizes result in the generation of different sizes of voids in the water channel [26]. The compressed air passed through a flow rate meter and a needle valve. The needle valve was used to isolate the back pressure from the coolant channel to the flow rate meter and was also used to control the flow rate. The flow rate meter, which had a scale reading in percentage, was calibrated to provide an absolute air flow rate indication for bubble generation. This was done using a test meter manufactured by the American Meter Company.

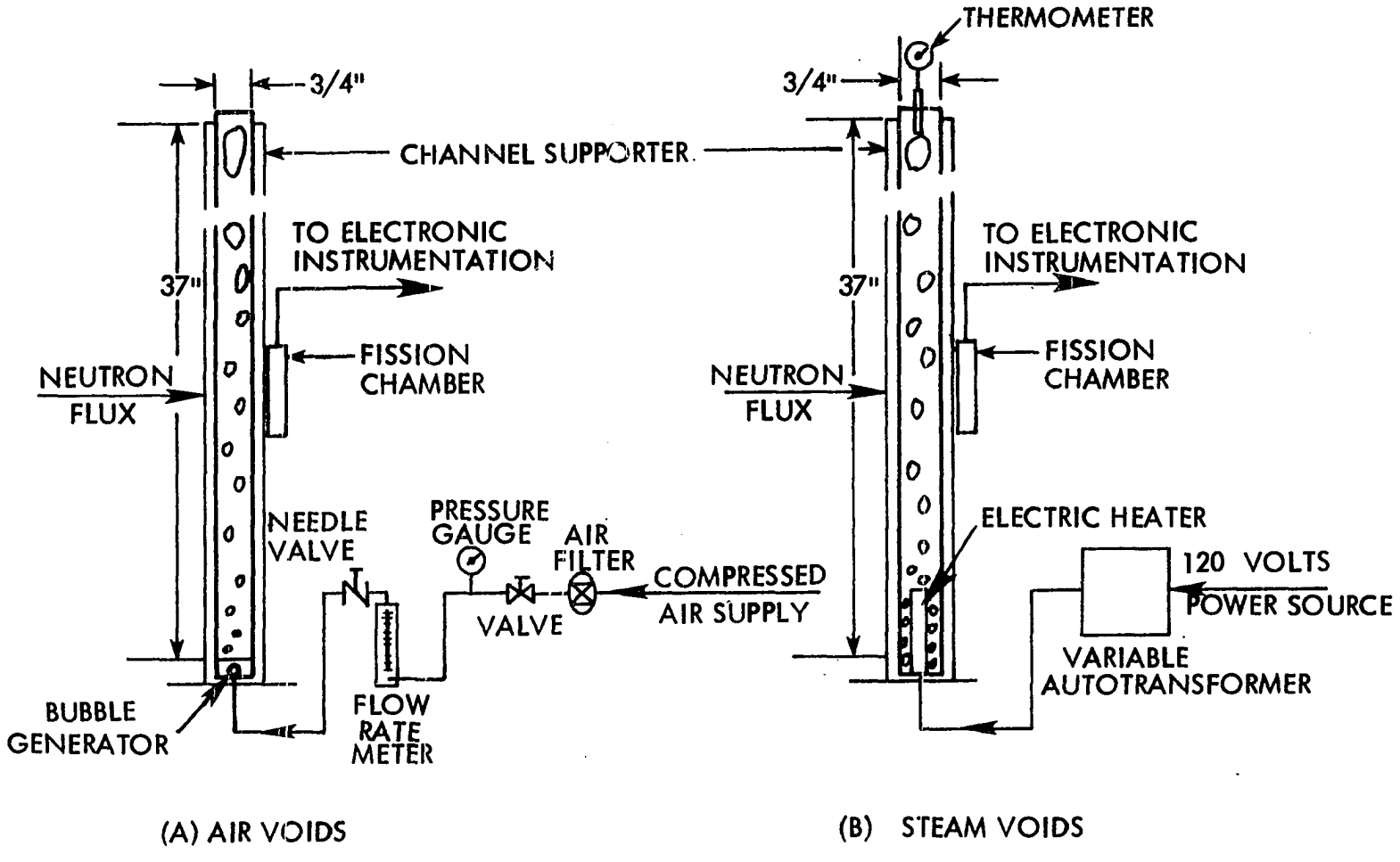

Fig. 5. The coolant void test section with neutron detector

For steam void generation, an electric heater with 20 ohms internal resistance and 2 kw rated power was used. The test section assembly with steam voids is shown in Fig. 5(b). The heater power was controlled by a variable auto-transformer with the range from 0 to 140 volts. A thermometer was placed on top of the channel to check for the saturation condition of boiling water.

For a visual study and to compare the results by the photocell technique with those of the neutron detector, a plexiglas channel was constructed having the same dimensions as the aluminum channel.

B. The Noise Signal Detection System

To detect the noise signal, two detection systems were used. One was the system with a neutron detector, and the other utilized a light source and photocell. The latter was used to compare the results with those from the neutron detector.

1. The system with the neutron detector

Fig. 6 shows the detection system for void fluctuations with a fission chamber as the neutron detector. The thermalized neutron flux from the thermal column of the Ames Laboratory Research Reactor (ALRR), which is a 5 mw enriched uranium-heavy water reactor, was used as the radiation source. A beam shutter was designed to stop the neutron flux when the experiment was not in operation. A Type WL-6376 fission chamber manufactured by Westinghouse Electric Co. was used in the current-mode as a neutron detector. An operating voltage of 400 volts for the detector was supplied by a Fluke 412B high voltage supply. The current generated by the neutron detector was measured from a high-sensitive picoammeter. The picoammeter

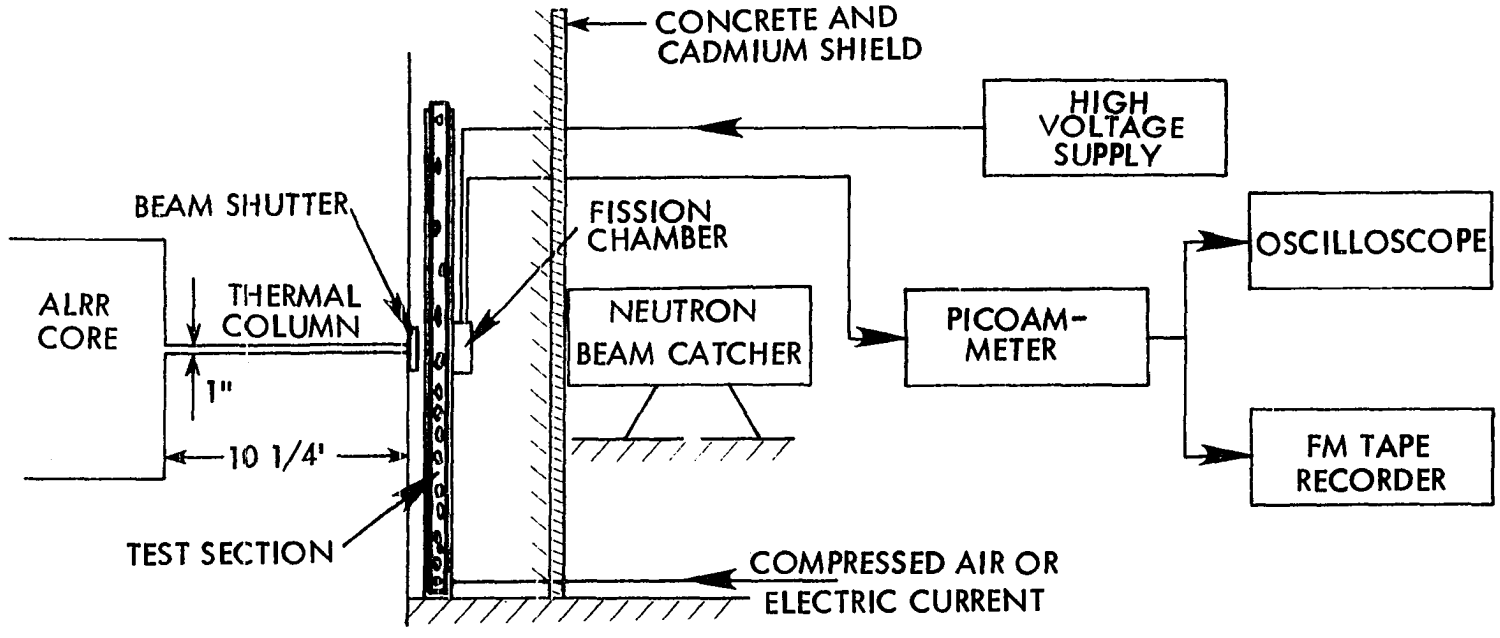

Fig. 6. Noise detection system with neutron detector

used in the experiment was a Keithley Instruments, Inc. Model 417. The d-c currents measured in the picoammeter can be removed using the current suppression circuit provided in the instrument. The noise signals were then taken from the voltage output of the picoammeter and recorded on low-noise magnetic tape by the PI-6200 FM tape recorder manufactured by the Precision Instrument Co. After noise signals were recorded on the magnetic tape, they were then analyzed or stored for later analysis.

2. The system with the photocell detector

In order to compare results obtained from the neutron detector, another system using a photocell detector was also designed. The neutron flux was replaced by a light source as shown in Fig. 7. A commercial selenium solar cell, which is sensitive to the light source and is capable of producing a 0.5 volt maximum voltage, was used as a photocell detector. The presence of voids in the coolant channel changes the intensity of light passing through the water medium and generates noise signals. An operational amplifier was used to amplify the noise signals. The void fluctuating signals were then recorded on the magnetic tape. In order to prevent the environmental light source from interfering with the void fluctuation measurement, dark paper was wrapped around the channel as a shield.

The light source for the selenium solar cell was a focused flash light bulb powered by a 1.5 volt battery. Since the voltage of the battery will decrease with time, care was taken to check the voltage reading of the battery constantly during the experiment.

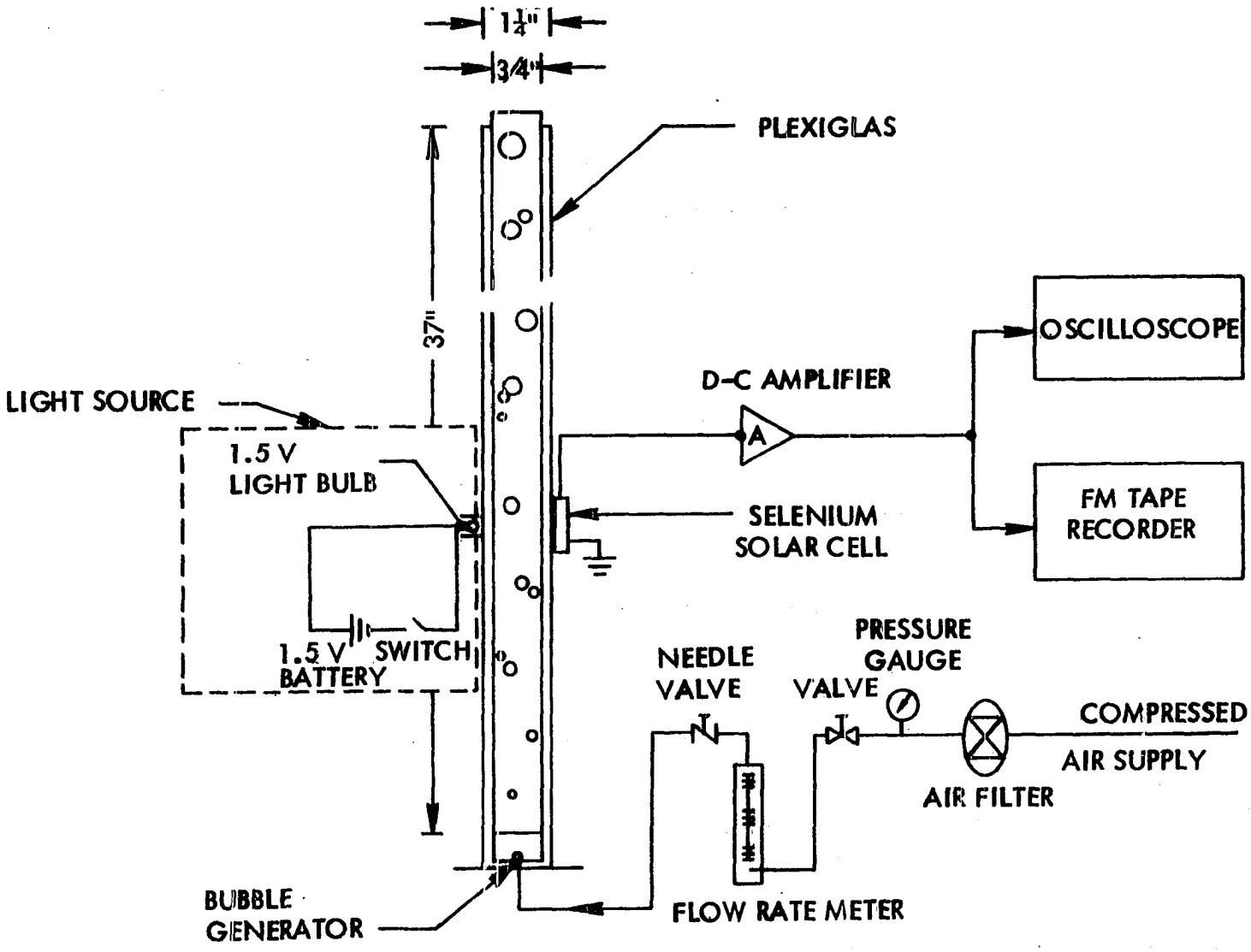

Fig. 7. Noise detection system by photocell detector

C. The Data Analysis System

1. Noise signal analysis system

Appropriate techniques for the acquisition and processing of random data are heavily dependent upon the physical phenomenon represented by the data and the desired engineering goals [46]. To analyze the noise signals in this study, the analysis system shown in Fig. 8 was designed for the digital computation. Noise signals, recorded on the tape, were played back from the FM tape recorder. The adjustable second order output filter in the tape recorder served to suppress the higher frequency components (anti-aliasing filtering) which were not of interest in the analysis. An off-set circuit was used to provide a positive noise signal level for the analog to digital converter (ADC). It included an operational amplifier, a potentiometer, and a -10 volts voltage source. The off-set level was varied between 0 and 8 volts depending on the amplitude of the input noise signal.

The ADC used in the analysis system was a Model 8050 manufactured by the Geoscience Nuclear Co. It was designed for multi-applications. For digitizing analog noise signals, a coincidence input which generates the sampling frequency is necessary. A BNC Model BH-1 tail pulse generator was used for this purpose.

The sampling frequency, f_s, has to be at least twice the cut-off frequency, f_c, of the input noise signals. The frequency, $2f_c$, is called the Nyquist frequency and is applied to avoid aliasing errors during signal digitization. Many sampling frequencies were tried, and an optimized value of $2.5f_c$ was selected in compromise with the available data analysis system and reasonable statistical results.

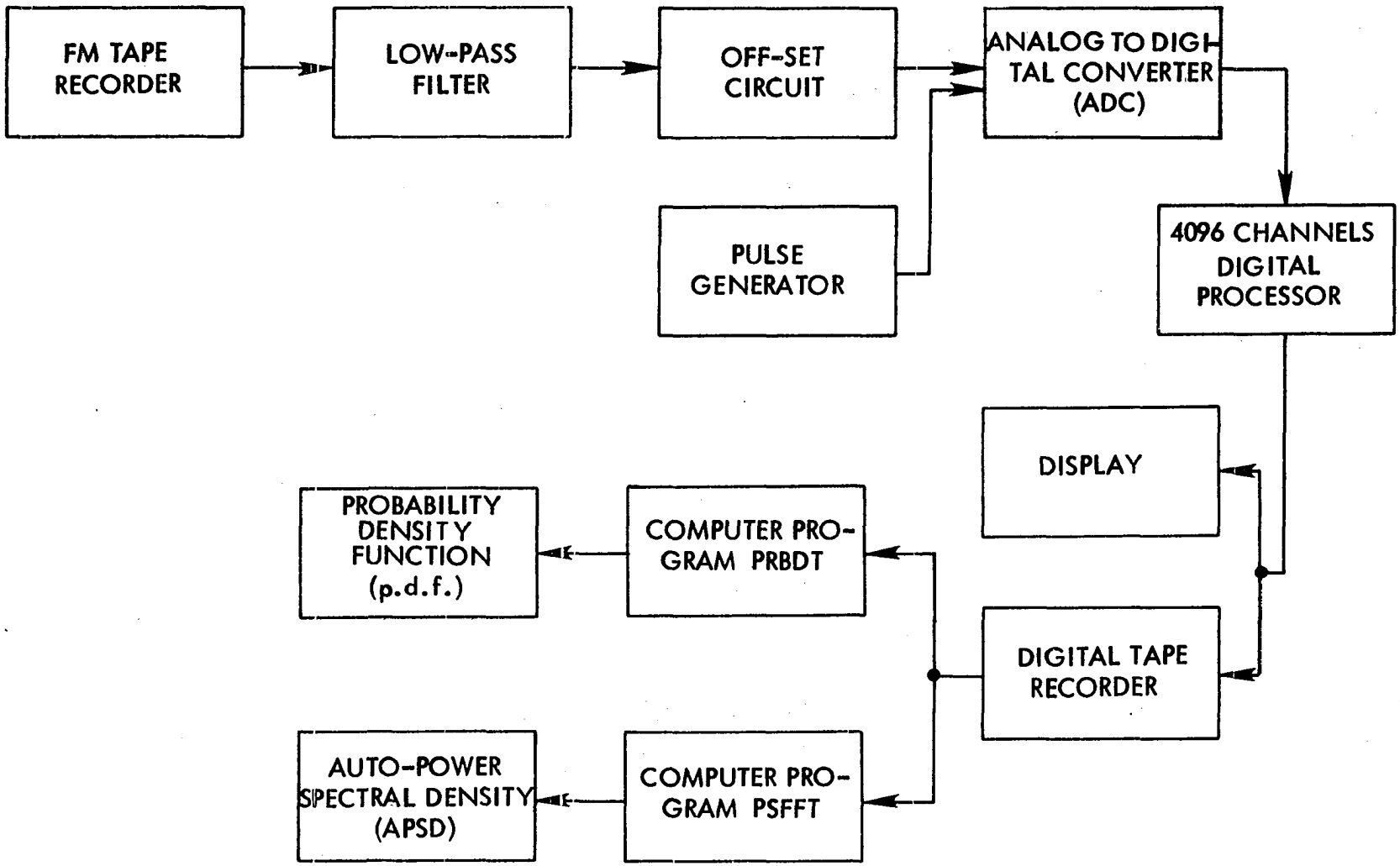

Fig. 8. Block diagram of the data analysis system

After the noise signals were digitized by the ADC, the data were stored in a 4096 channels Model 7000 Digital Processor manufactured by the Geoscience Nuclear Co. A display was used to check the digitized data before recording on the digital magnetic tape.

The digitized data on the tape were then supplied to the computer program PRBDT for probability density function calculations or to the PSFFT program for the evaluation of the auto-power spectral density.

2. The computer programs

a. PRBDT The PRBDT program is used to calculate the probability density function (PDF) of a sample time history record. A subroutine TAB1, which is in the IBM PL/1 Scientific Subroutine Package (SSP), was used as a major subprogram for the calculation. The PRBDT tabulates, for the magnitude of the signal record, the frequency, percent frequency, and the PDF over given class intervals. It also calculates the total, mean, standard deviation, minimum, and maximum. The interval size is determined by the number of intervals and was selected to be about 30% of the standard deviation for the purpose of sorting the random sample record. The program is listed in Appendix C.

b. PSFFT The PSFFT program, also written in PL/1 language, was used to calculate the auto-power spectral density (APSD) functions. Digital input signals were supplied from magnetic tapes. The subroutine FFT (fast Fourier transform), in the IBM PL/1 SSP, is used as a major technique for the Fourier transform in the program for the power spectral density calculation.

The flow diagram of PSFFT is shown in Fig. 9. Due to the introduction of the off-set circuit, a d-c component was induced on the data file. It was necessary to remove the d-c component before performing the APSD analysis. In order to reduce the side lobe leakage of the finite time interval in the FFT, a tapering technique of the original random time series at each end is required [46,55]. Several "window functions" are available for this, see for example Refs. 46 and 55. The cosine taper was selected for the PSFFT in this work.

The APSD, after application of the fast Fourier transform, is essentially a raw estimate, and the standard error ϵ is expressed as [46,55]:

$$\epsilon = 1/(BeT)^{\frac{1}{2}} \tag{4.1}$$

where T = finite time interval of a sample data record,

and Be = bandwith of the estimate.

For the fast Fourier transform, Be is equal to 1/T, and each estimate is governed by a chi-square distribution with 2 degrees of freedom [46]. This implies that

$$\epsilon = 1/(\frac{1}{T} \times T)^{\frac{1}{2}} = 100\%. \tag{4.2}$$

A 100% standard error is not acceptable for practical applications. Two averaging techniques, frequency smoothing and segment averaging, were used to reduce the standard error in Eq. (4.1) and also to save computation time.

The combined averaging using both frequency smoothing and segment averaging was applied in the PSFFT. The number of neighboring frequency components to be averaged, L, for frequency smoothing depends on the required accuracy, the desired bandwidth, and the available computation

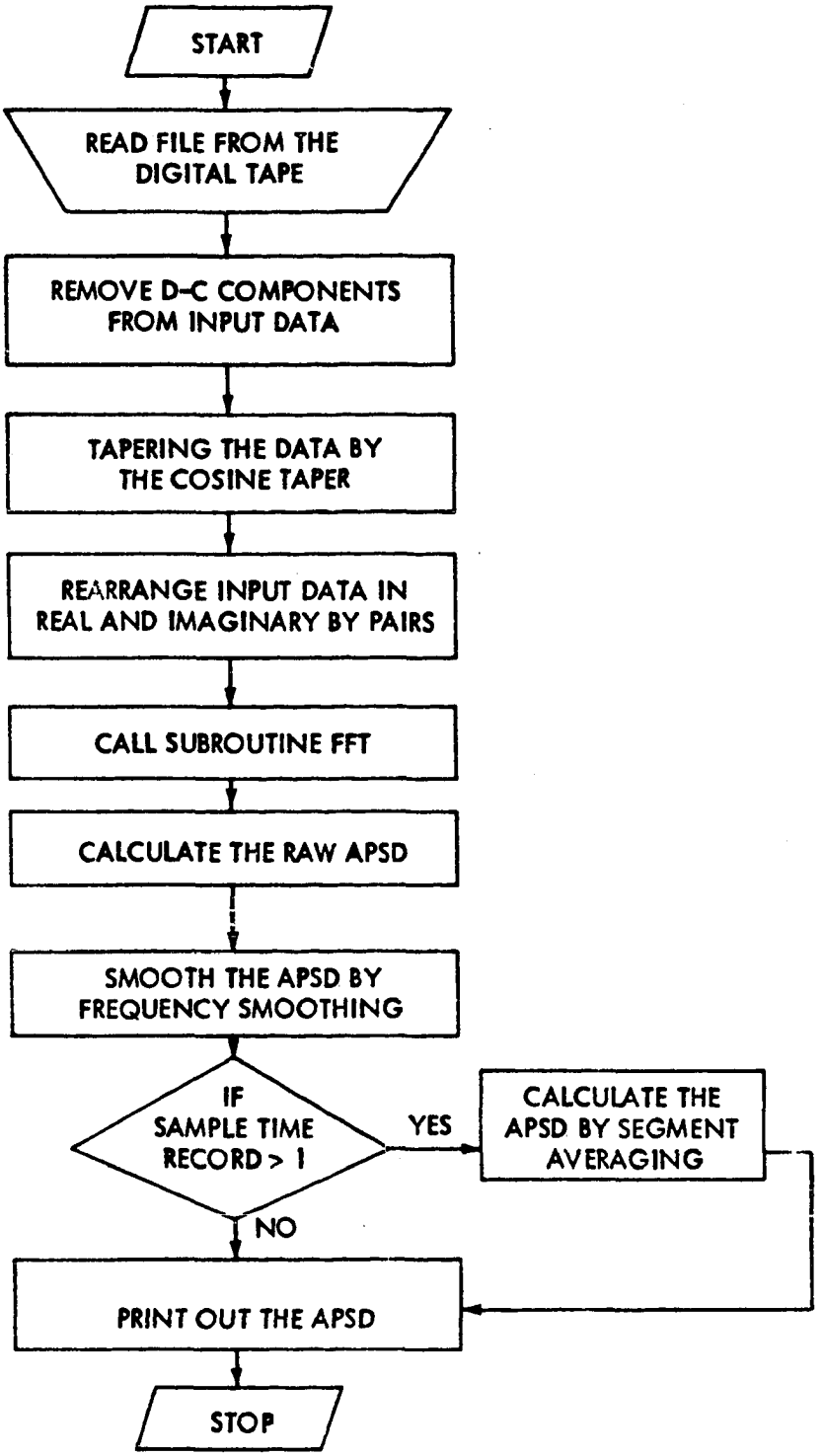

Fig. 9. Flow diagram of the PSFFT

time. For the PSFFT, the frequency range between 0.3 Hz and 100 Hz was divided into eight separate parts for frequency smoothing, and the desired bandwidth varied from 0.2 Hz at 0.3 Hz to 10 Hz at 100 Hz. The L's were then determined by the selected bandwidth, Be', and calculated from the equation

$$L = Be'T. \tag{4.3}$$

Segment averaging is based on the results from N separate time slices, where each time slice is of length T. In the PSFFT, the number of separate time slices was also supplied depending on the required accuracy. In this study, eight separate time slices were in general used for the power spectral density calculation. The number of time slices used was based on computer time and statistical considerations.

The resulting power spectral density, with combined averaging, will have n degrees of freedom, and the standard error is given by [46]

$$n = 2LN \tag{4.4}$$

$$\varepsilon = (1/LN)^{\frac{1}{2}}. \tag{4.5}$$

The standard error was calculated and printed out for each power spectral density evaluation. The complete PSFFT program is listed in Appendix D.

V. EXPERIMENTAL PROCEDURE

A. Neutron Flux and Cadmium Ratio Measurements

Before taking any noise measurement of void fluctuations, it is necessary to estimate the intensity and the cadmium ratio of the neutron flux from the thermal column of the reactor. Results of these measurements are used to check if the neutron flux is well thermalized and if the neutron intensity is adequate for the neutron detection system.

The neutron flux with a one-inch diameter beam was taken from the thermal column of the ALRR, which was normally at 5 Mw full power operation. The neutron flux is thermalized when it passes through the thermal column. The intensity and the cadmium ratio of the neutron flux were measured by using the technique of gold foil irradiation. The results are listed in Table 1.

For the well-collimated neutron beam as used in this study, an intensity of 10^8 neutrons/cm^2-sec is adequate for the neutron detector. The cadmium ratio of approximately 134 indicates the neutron fluxes are well thermalized.

Table 1. Results of the neutron flux measurement at the surface of the thermal column of ALRR[a]

Run no.	Thermal neutron flux ϕ_o, n/cm^2-sec	Cadmium ratio Rcd	Average values ϕ_o, n/cm^2-sec	Rcd
1	1.03×10^8	136.4	0.992×10^8	134.3
2	0.954×10^8	132.3		

[a]Operated at 5 Mw.

B. Flow Rate Calibration

The flow rate meter used in this experiment reads in percentage of full scale and has to be calibrated to obtain the actual air flow rate. A test meter connected to the flow rate meter was used for this purpose. The air flow rate was calculated based on the total air flow reading in the test meter and the elapsed time to the reading. A least-square fit was applied to the data to obtain the calibration curve shown in Fig. 10.

C. Testing of Noise Signals for Stationarity

The stationarity of noise signals is an important condition for noise analysis both in the PDF and APSD calculations. The processing techniques discussed in Chapter III are, for the most part, applied to stationary data only [46]. To verify the stationarity of the noise signals, the root mean square (RMS) value versus time was determined. A circuit was wired on the TR-48 analog computer to perform the measurements. The constant RMS values shown in Fig. 11 indicate that the noise signals for this study are stationary and thus the processing techniques of stationary data apply.

D. Background Noise Measurements

Before any data run of void fluctuations was made, the characteristics of the background noise signal were determined. This background signal consists of instrumentation noise (detection and electronic), branching process noise, and other power noise. The electronic instrumentation noise was measured by closing the beam shutter. The detection, branching process, and power noise were detected by opening the beam shutter without voids in the coolant channel. The d-c component of the background was suppressed and read from the picoammeter. The noise signal with zero mean was

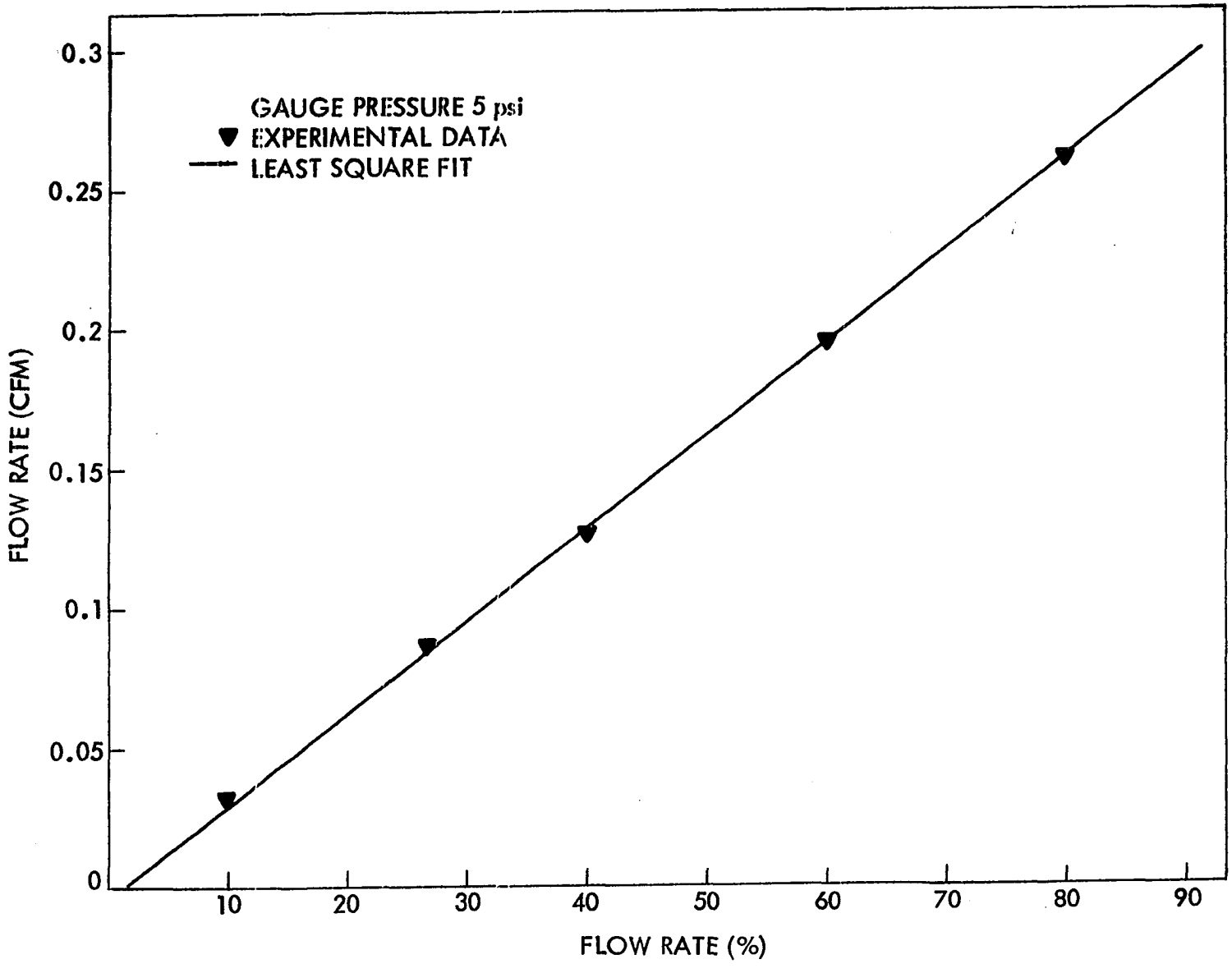

Fig. 10. Calibration of air flow rate reading

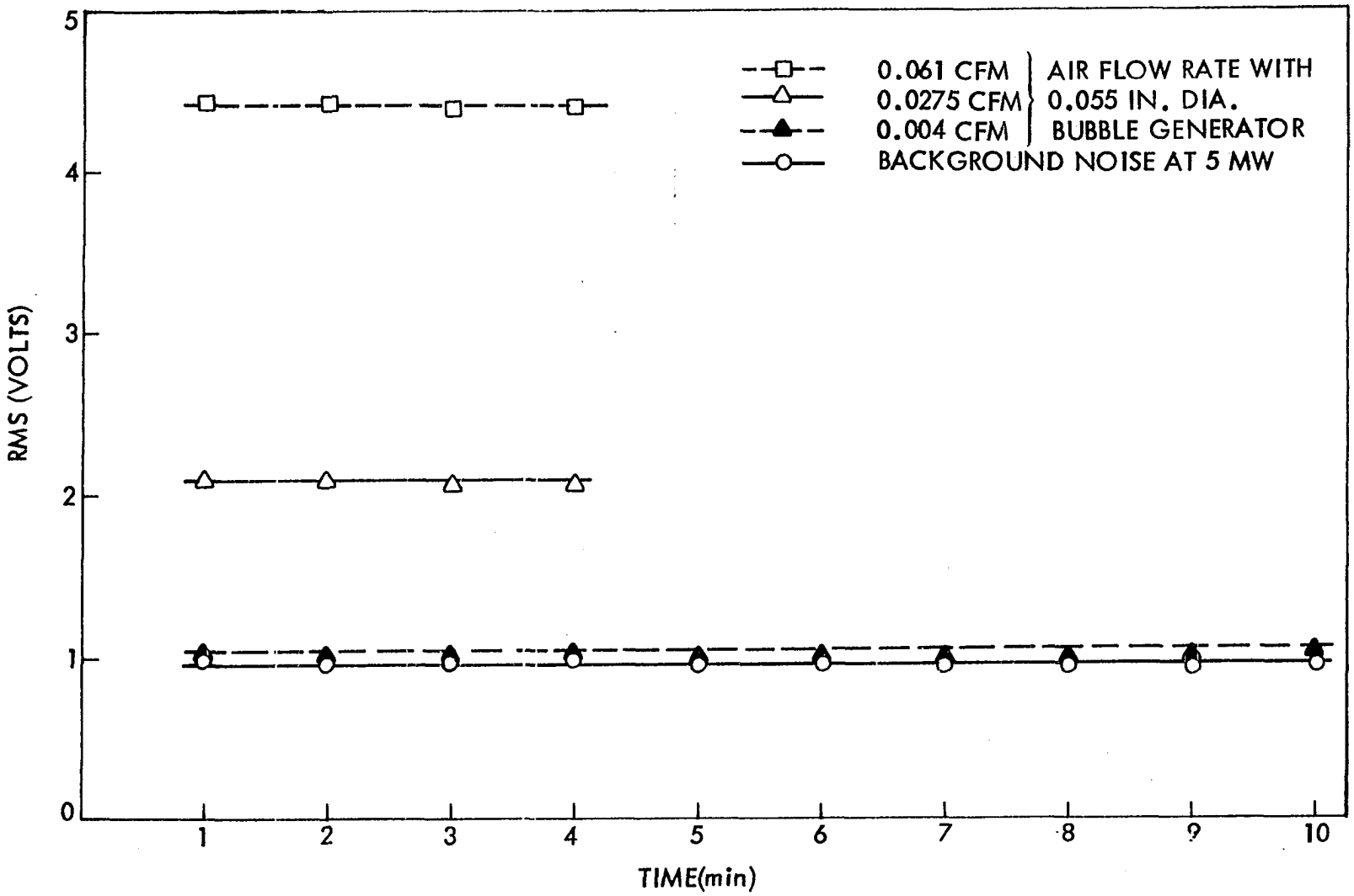

Fig. 11. Root mean square values of noise signals vs time

then recorded on the magnetic tape and used for comparisons with void signals.

E. Air Void Fluctuation Measurements

To study the air void fluctuation, air voids were generated by the bubble generator. The void characteristics were controlled by the bubble generator size, air flow rate, and water head in the coolant channel. Prior to data collection, air bubbles were supplied into the coolant channel for a few minutes. It is assumed that water and air in the channel are in an equilibrium state after a short time interval.

For the detection system with the neutron detector, noise signals were extracted from the picoammeter after suppressing and recording the d-c components and then recorded on the tape recorder at a tape speed of 3.75 inches per second (bandwidth 1000 Hz). The noise signals obtained from the photocell detector were directly recorded on the magnetic tape. No suppression of d-c components is needed in this case because of the rather low signal level.

The steps for air void fluctuation measurements were the following:

(1) Fix the size of the bubble generator and the detector position, change the air flow rate by flow rate meter, and record the noise signals.

(2) Fix the size of the bubble generator and the air flow rate, change the detector position by moving the coolant channel up and down, and record signals.

(3) Fix the air flow rate and the detector position, change the size of the bubble generator, and measure noise signals. The above

three steps were completed using a full tank of water in the channel.

(4) Lower the water head to 24" high and repeat steps (1), (2), and (3).

(5) Lower the water head to 14" high and repeat steps (1), (2), and (3).

F. Steam Void Fluctuation Measurements

In order to compare the results of void fluctuations of air-water mixtures with those of steam-water mixtures, steam voids were generated by an electric heater placed at the bottom of the coolant channel. The noise signals of steam voids were measured by the fission chamber and recorded from the output of the picoammeter. The characteristics of steam voids were controlled by the power supplied to the electric heater. The steps for steam void measurements were:

(1) Fix the heater power, change the detector position by moving the coolant channel up and down, and record noise signals.

(2) Fix the detector position, change the heater power by adjusting the variable auto-transformer, and record signals on tapes.

G. Data Processing

Once the data were recorded on the magnetic tape, the remaining steps for the data analysis were:

(1) Digitize the data by the ADC and store in the digital processor and then record on the digital tape. The process here is shown in the block diagram of Fig. 8.

(2) Read the digital tape into the PRBDT and PSFFT programs for the probability density function and the power spectral density calculation, respectively.

(3) Print out and analyze the results.

The output filter of the tape recorder was set at 100 Hz for the processing of recorded signals.

H. Average Void Fraction Calculation

In order to see how the void fluctuations are affected by the average void fraction in the coolant channel, the average void fractions were also calculated. They were evaluated based on the air flow rate and the terminal velocity of voids in the coolant channel [26]. The method of evaluation and results of void fractions are listed in Appendices A and B, respectively. Average void fractions of approximately 0.5% to 7.5% were obtained for the experiment.

VI. DATA AND RESULTS

A series of data runs have been carried out in order to study the aspects, previously discussed, of void fluctuations in a coolant channel. The experimental conditions were based on changes of various parameters of air and steam voids. In case of the air voids, both bubble generator hole size and air flow rate were varied to change bubble size and generation rate. For steam voids, heater power was varied to change bubble characteristics. The values of the parameters used in this study are indicated in the tables and figures of the experimental results. The detector positions for air and steam voids were selected as shown in Fig. 12.

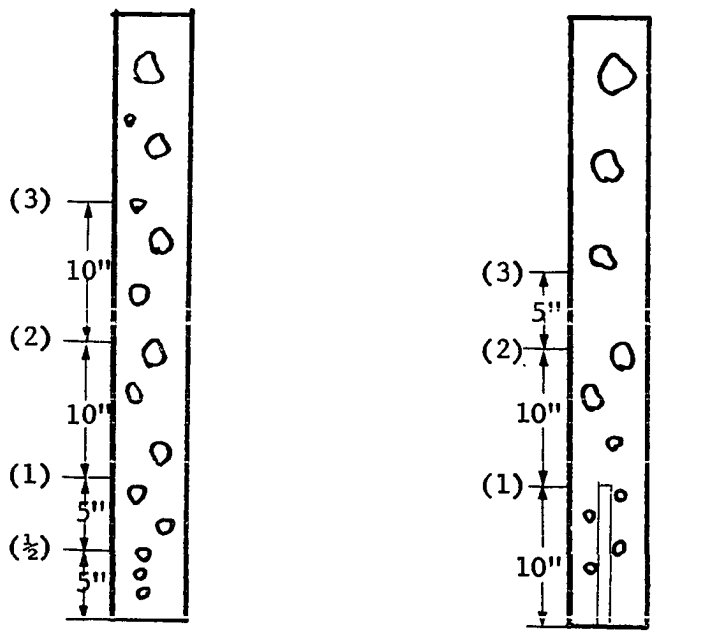

(a) air voids (b) steam voids

Fig. 12. Detector positions

A. Visual Observations

Fig. 13 shows typical photographs of void motion in the coolant channel at different air flow rates with a 0.055 inch diameter bubble generator.

Fig. 13. Visual observations of void fluctuations with a 0.055 in. dia. bubble generator and different air flow rates

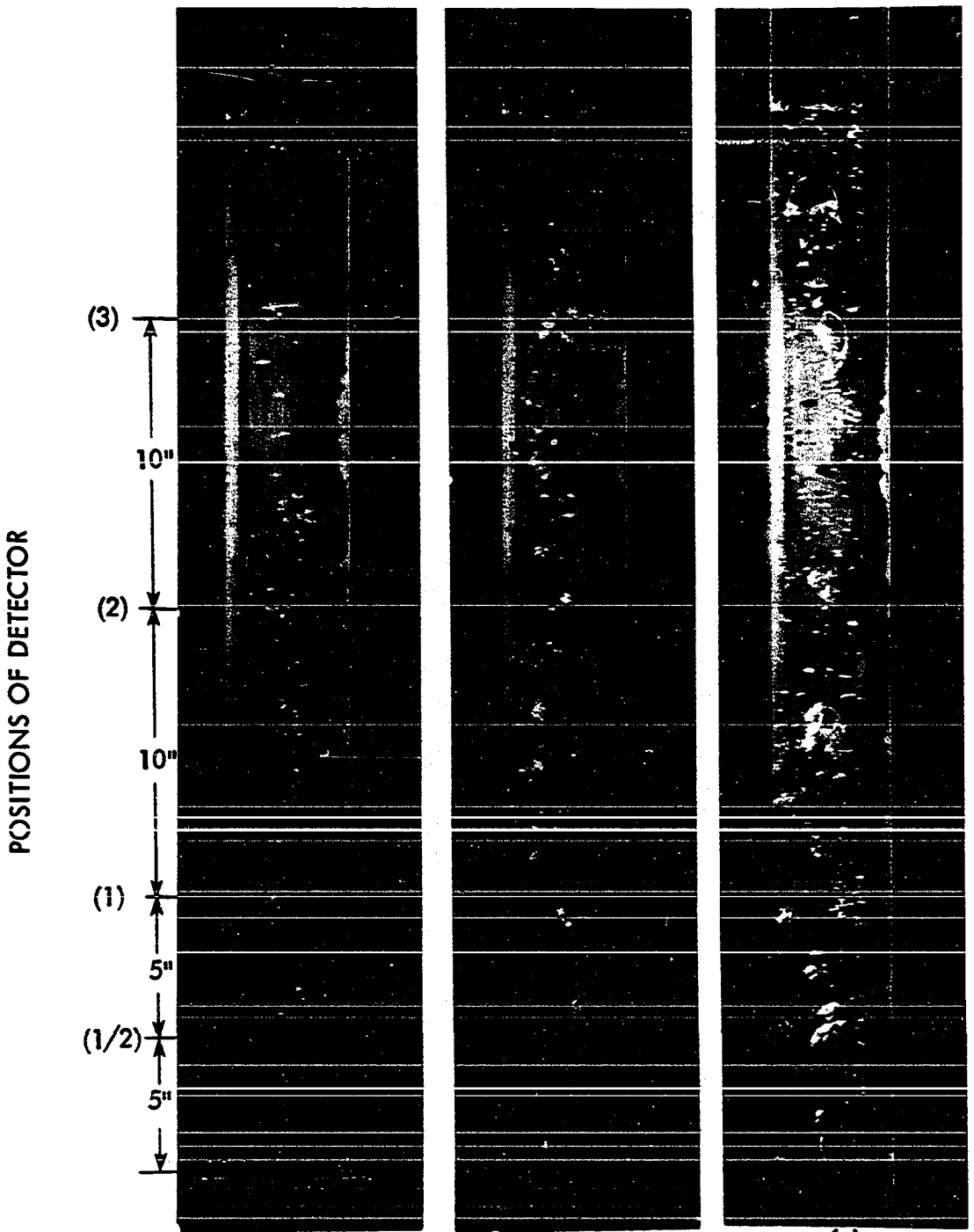
POSITIONS OF DETECTOR
(3)
10"
(2)
10"
(1)
5"
(1/2)
5"
(a)
(b)
(c)
Air flow rate
Bubble generator dia.
0.004 CFM
0.055 in.
0.0275 CFM
0.055 in.
0.061 CFM
0.055 in.

When the air flow rate increases, the void size as well as the void motion will change as observed in the figure. The flow regime in two-phase flow would tend to become slug flow as shown in Fig. 13(c) for high flow rate.

The noise signals due to air voids at different positions based on a fixed bubble size and air flow rate are compared in Fig. 14(A). The noise signals due to voids increase in amplitude as the neutron detector is moved along the coolant channel away from the bubble generator. Fig. 14(B) shows comparisons of steam voids with a 320-watt heater power. Both Fig. 14(A) and Fig. 14(B) show the same trend of the detector response. This gives a good indication that for these conditions the air-water mixture can be used to represent steam voids for the two-phase flow study.

The detector responses to different air flow rates and heater powers for a fixed bubble generator and detector are shown in Fig. 15. As in Fig. 14, similar trends are found for air and steam voids. Increasing the air flow rate or heater power results in an increased fluctuation amplitude.

B. Results of Probability Density Function Calculations

1. Experimental results

To study the distribution of amplitudes of noise signals, the probability density functions (PDF's) were calculated. The PDF of the neutron beam without air voids is compared with a Gaussian distribution in Fig. 16. These results are typical of the neutron detection processes. Figs. 17, 18, and 19 show the PDF's of the detector signals with air voids in the coolant channel for different flow rates but with the same 0.055-inch diameter bubble generator. The detector responses to void fluctuations at a

Fig. 14. Noise signals of air and steam voids at different positions

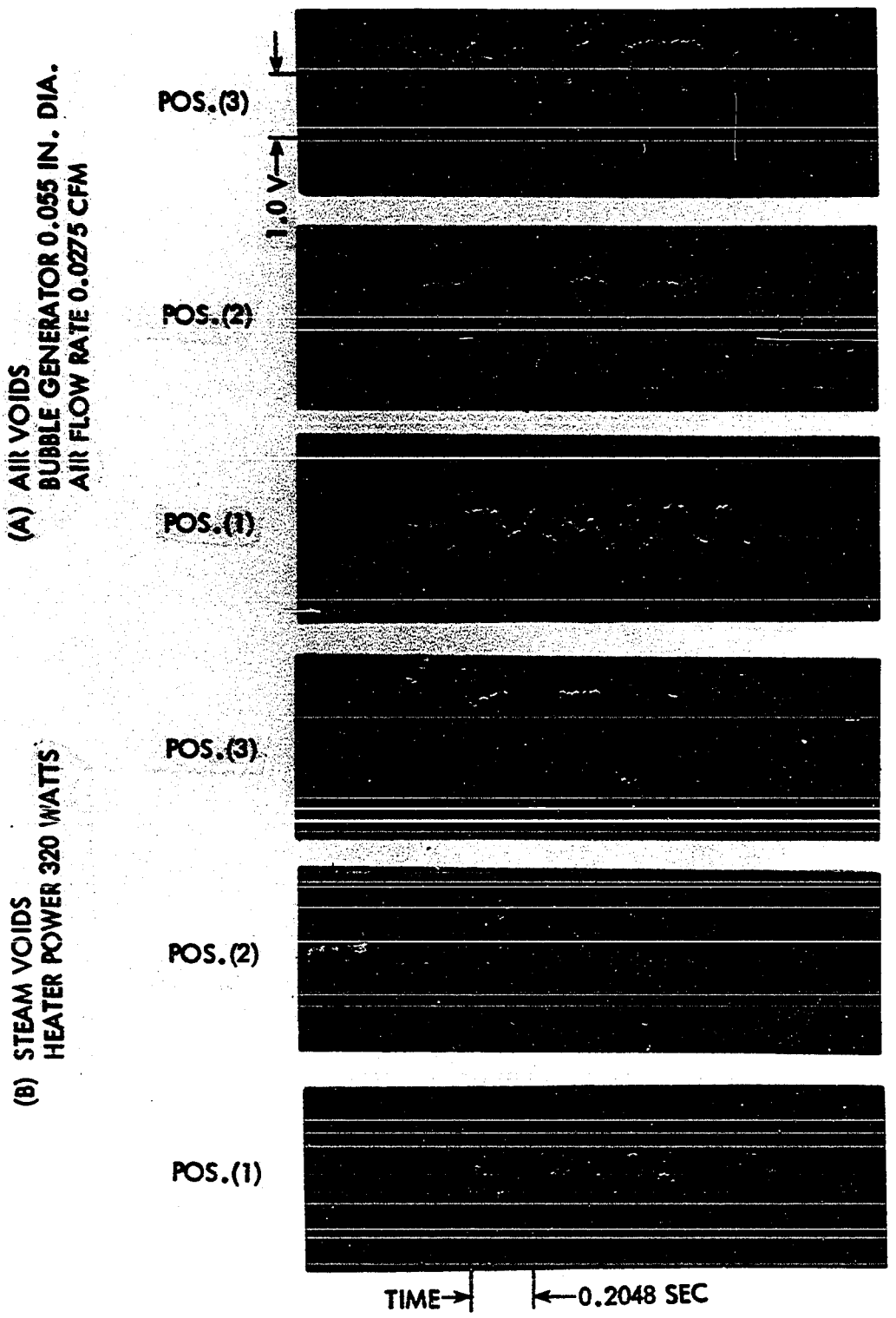
(A) AIR VOIDS
BUBBLE GENERATOR 0.055 IN. DIA.
AIR FLOW RATE 0.0275 CFM
POS.(3)
1.0 V
POS.(2)
POS.(1)
(B) STEAM VOIDS
HEATER POWER 320 WATTS
POS.(3)
POS.(2)
POS.(1)
TIME
0.2048 SEC

Fig. 15. Noise signals of air and steam voids at different flow rates and heater powers

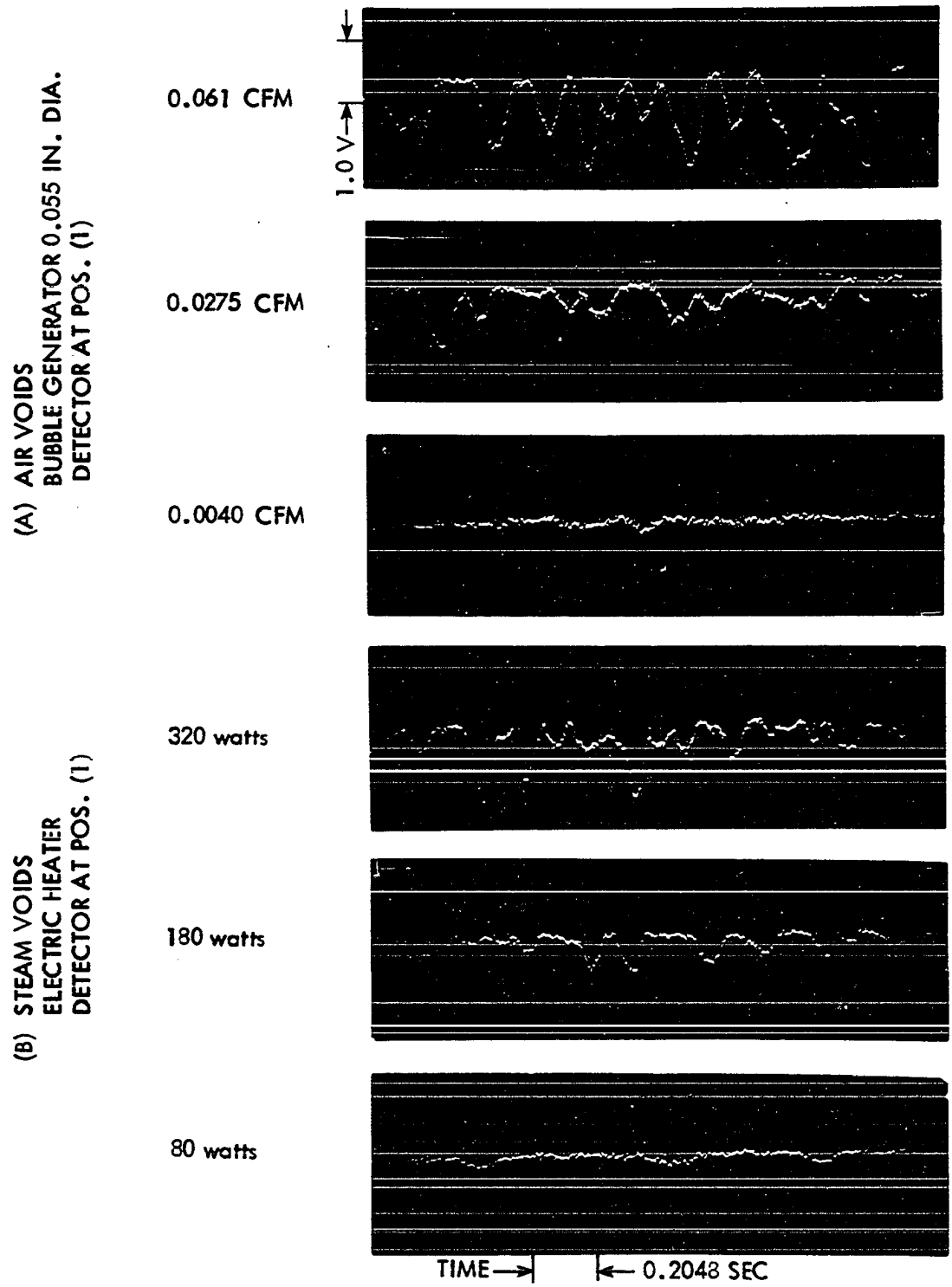
(A) AIR VOIDS
BUBBLE GENERATOR 0.055 IN. DIA.
DETECTOR AT POS. (1)
0.061 CFM
1.0 V
0.0275 CFM
0.0040 CFM
(B) STEAM VOIDS
ELECTRIC HEATER
DETECTOR AT POS. (1)
320 watts
180 watts
80 watts
TIME
0.2048 SEC

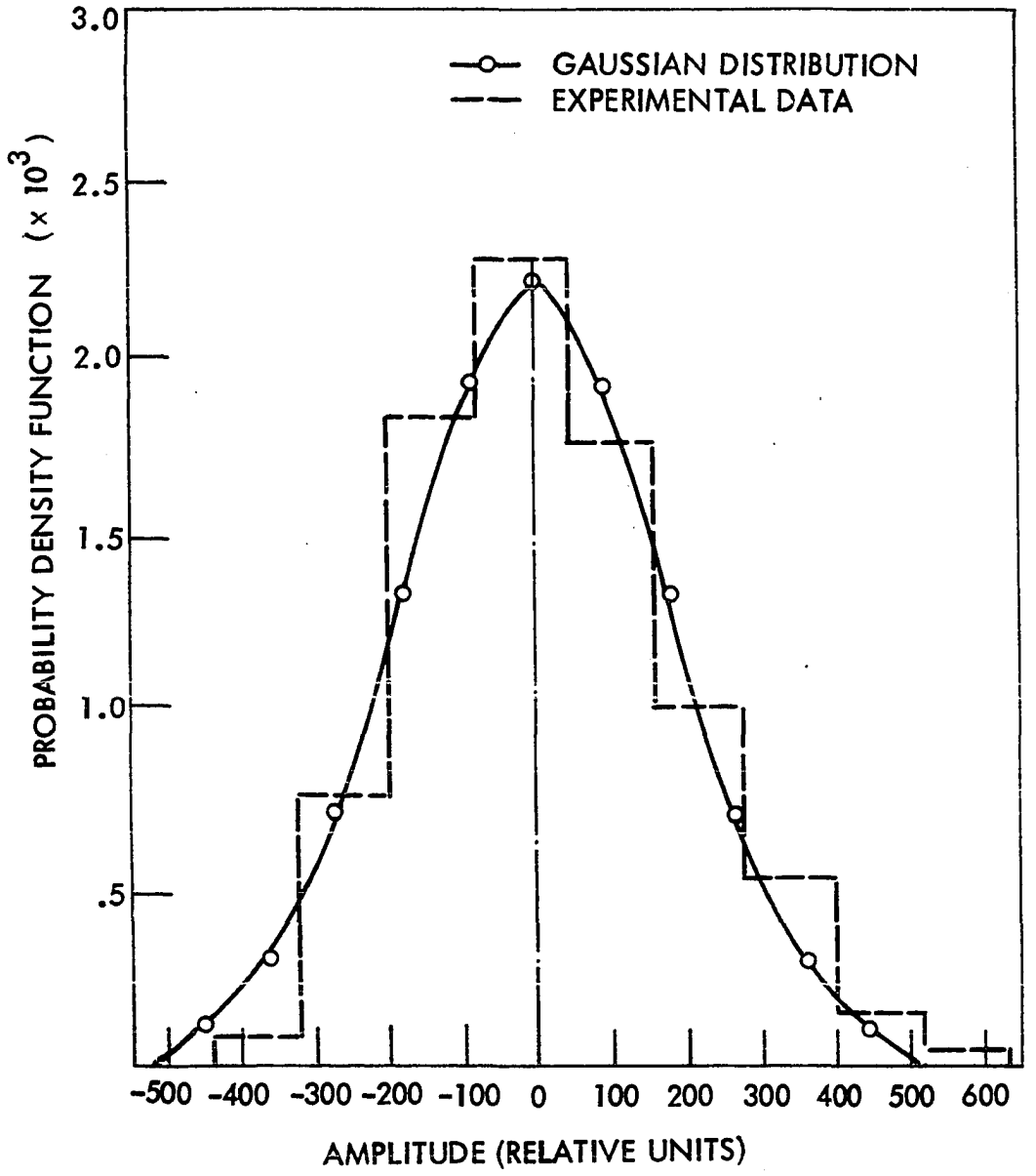

Fig. 16. Probability density function of the background noise source

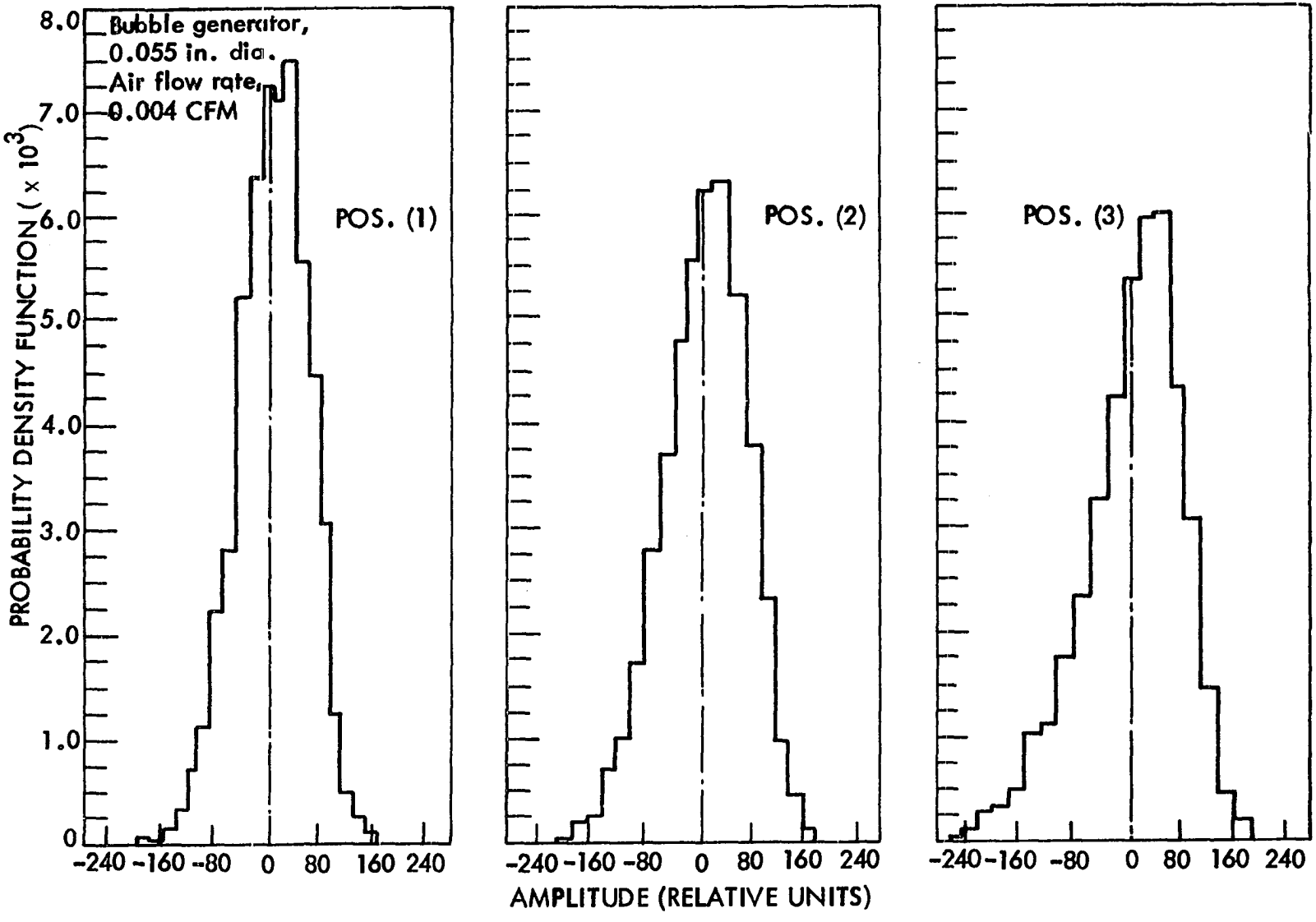

Fig. 17. Probability density function of air voids with a 0.055 in. dia. bubble generator and 0.004 CFM air flow rate

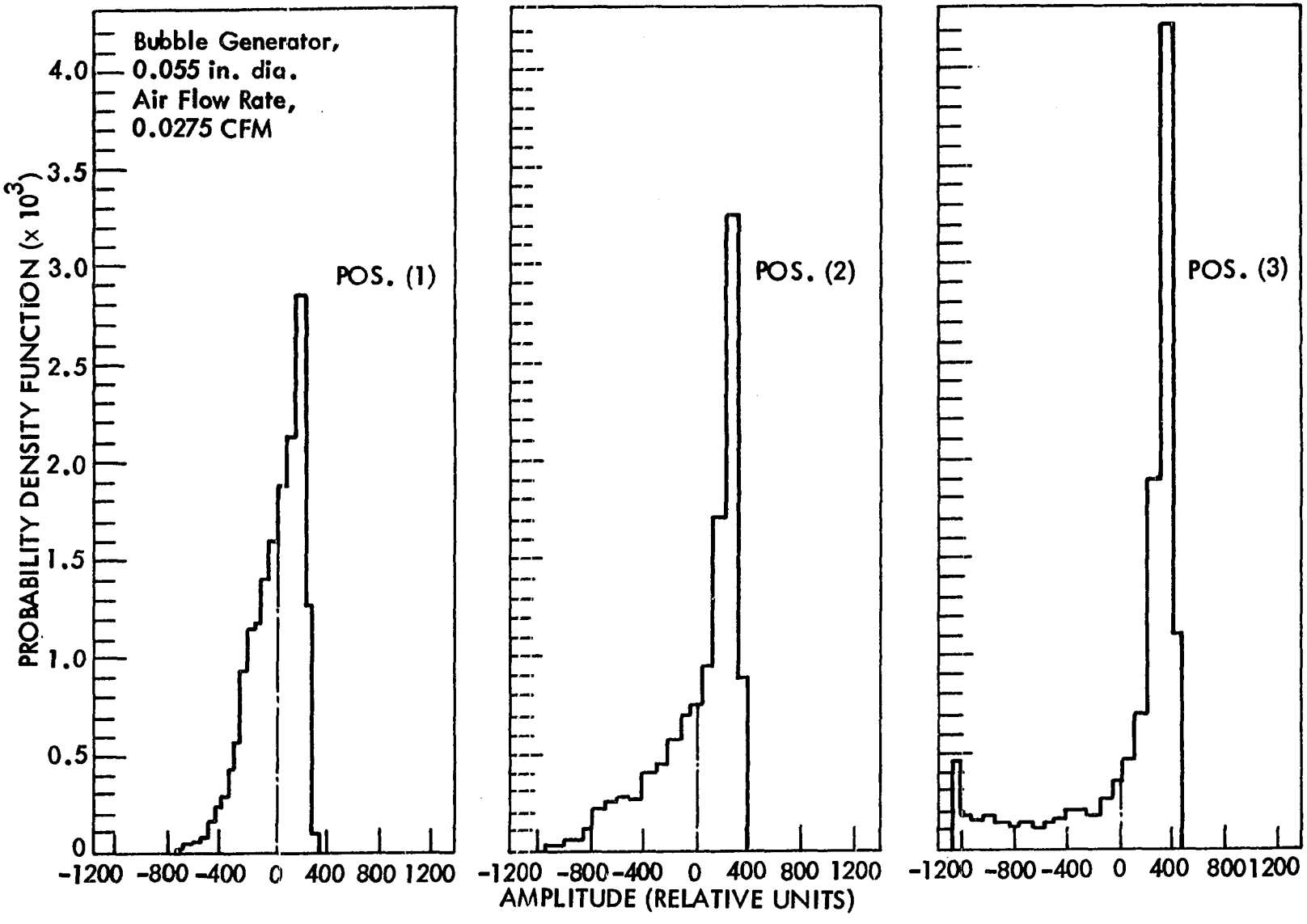

Fig. 18. Probability density function of air voids with a 0.055 in. dia. bubble generator and 0.0275 CFM air flow rate

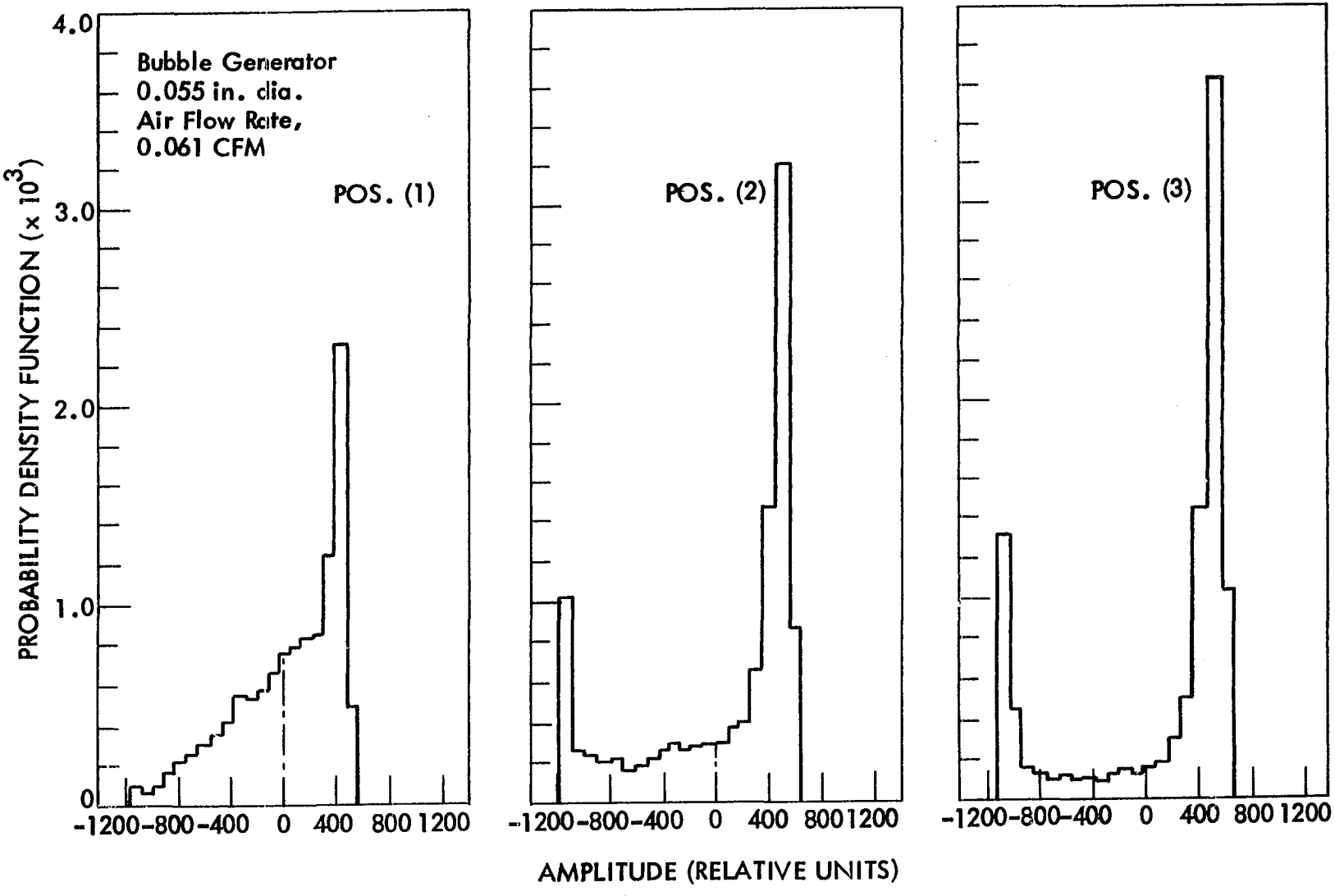

Fig. 19. Probability density function of air voids with a 0.055 in. dia. bubble generator and 0.061 CFM air flow rate

low flow rate, as shown in Fig. 17, indicate a linear detection process. A small fluctuation of voids in the coolant channel is also shown in this figure. Figs. 18 and 19 show unsymmetric probability density functions of noise signals when the flow rates increase. These results indicate the nonlinear process of void fluctuations in the system as well as the change in void fluctuations. The different PDF's along the coolant channel as shown in Figs. 17, 18, and 19 also give a clear indication of the space-dependent characteristics of voids.

Based on the same air flow rate of 0.0275 CFM but different bubble generator sizes, Figs. 17, 20, and 21 show that the void fluctuations are sensitive to the size change of the bubbles. As indicated in these figures, bubble size is one of the important factors affecting the characteristics of void fluctuations.

Figs. 22, 23, and 24 shows the PDF's of steam void fluctuations for 80 watts, 180 watts, and 320 watts of heat power, respectively. At the power levels of 180 watts and 320 watts, the entire channel was at saturation conditions, while at 80 watts the water temperature at the top of the channel was about 200° F. Small fluctuations of steam voids are shown in Fig. 22. At saturation conditions, Figs. 23 and 24 also show the difference of void fluctuations at different power level and the skewness of void signals in the system. The possible changes of flow regimes from bubble flow to partial slug flow are shown at POS. (2) and (3) of Fig. 24, as the PDF's change quite drastically.

The PDF of void fluctuations with a 0.055 in. diameter bubble generator and a flow rate of 0.0275 CFM, as measured with the photocell detector, is shown in Fig. 25. In comparison with the results of the neutron detec-

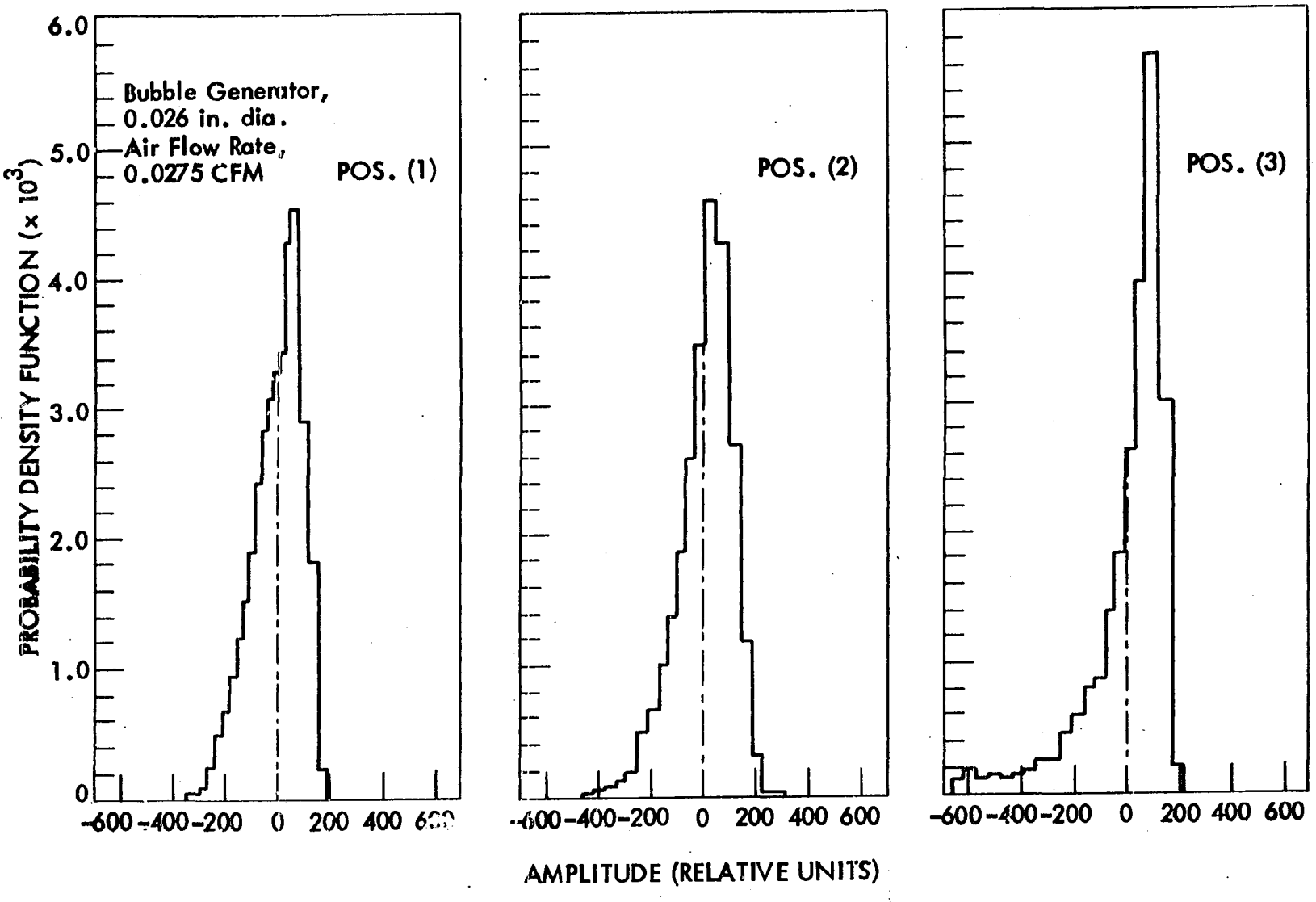

Fig. 20. Probability density function of air voids with a 0.026 in. dia. bubble generator and 0.0275 CFM air flow rate

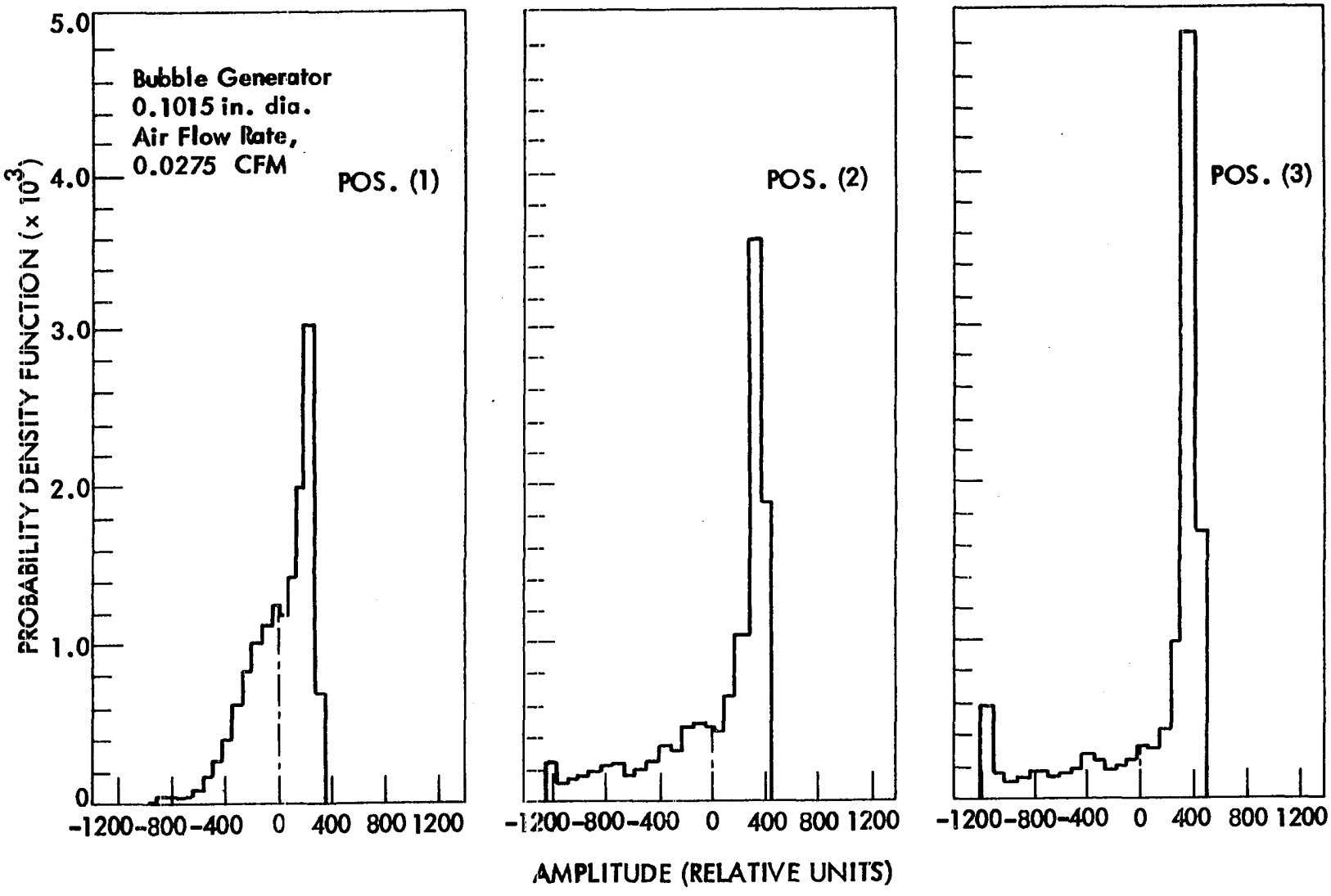

Fig. 21. Probability density function of air voids with a 0.1015 in. dia. bubble generator and 0.0275 CFM air flow rate

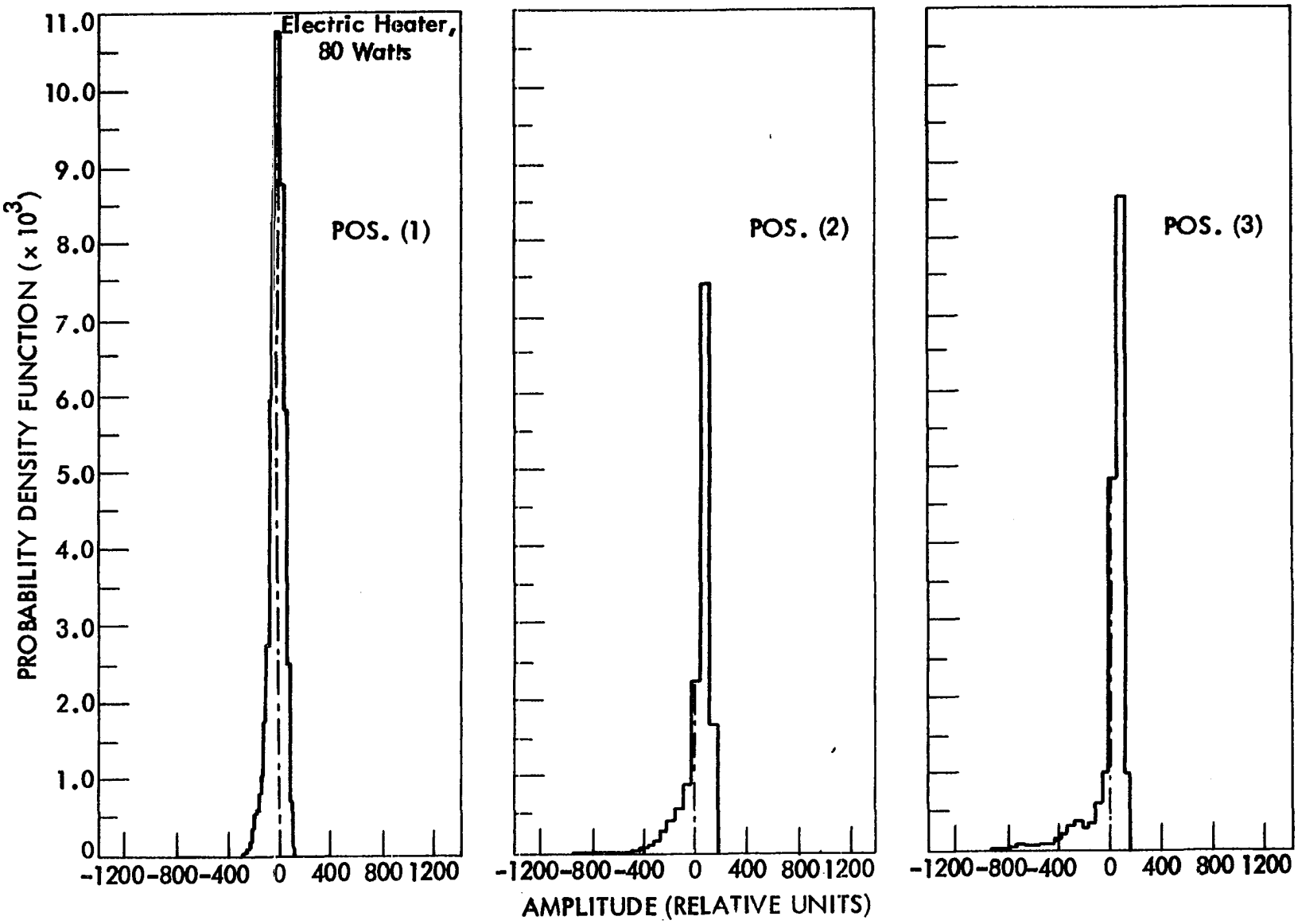

Fig. 22. Probability density function of steam voids with 80 watts of heater power

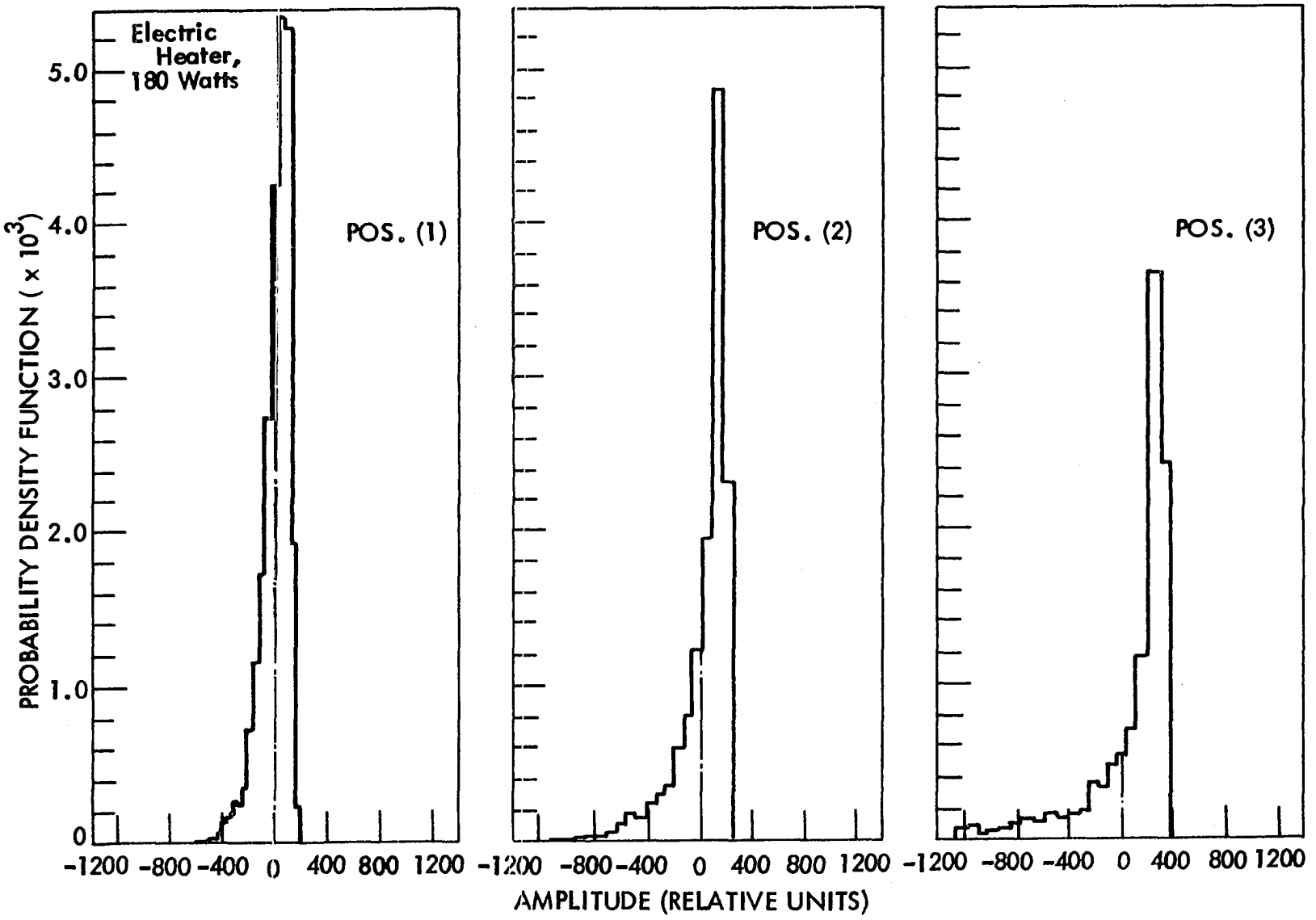

Fig. 23. Probability density function of steam voids with 180 watts of heater power

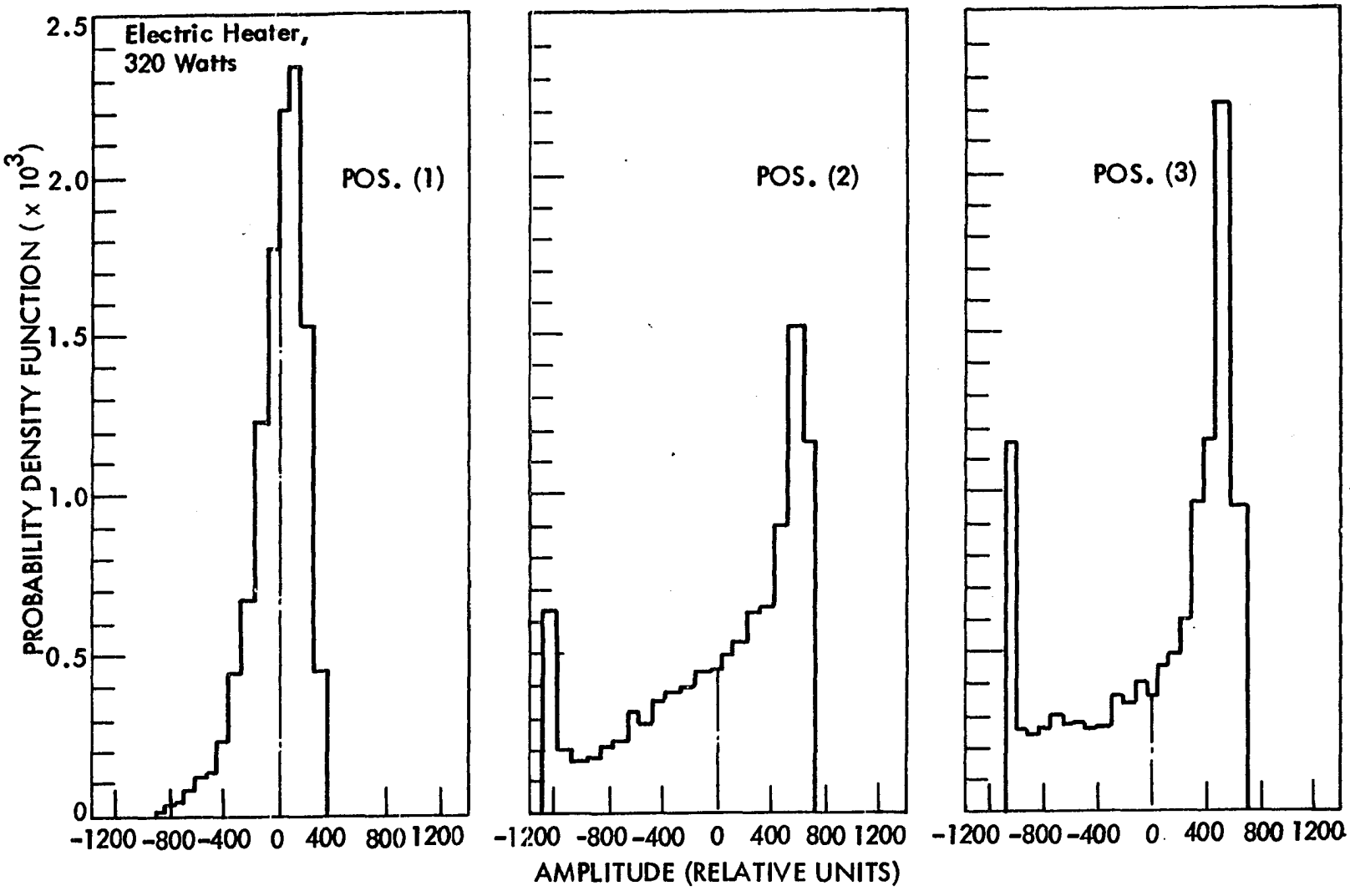

Fig. 24. Probability density function of steam voids with 320 watts of heater power

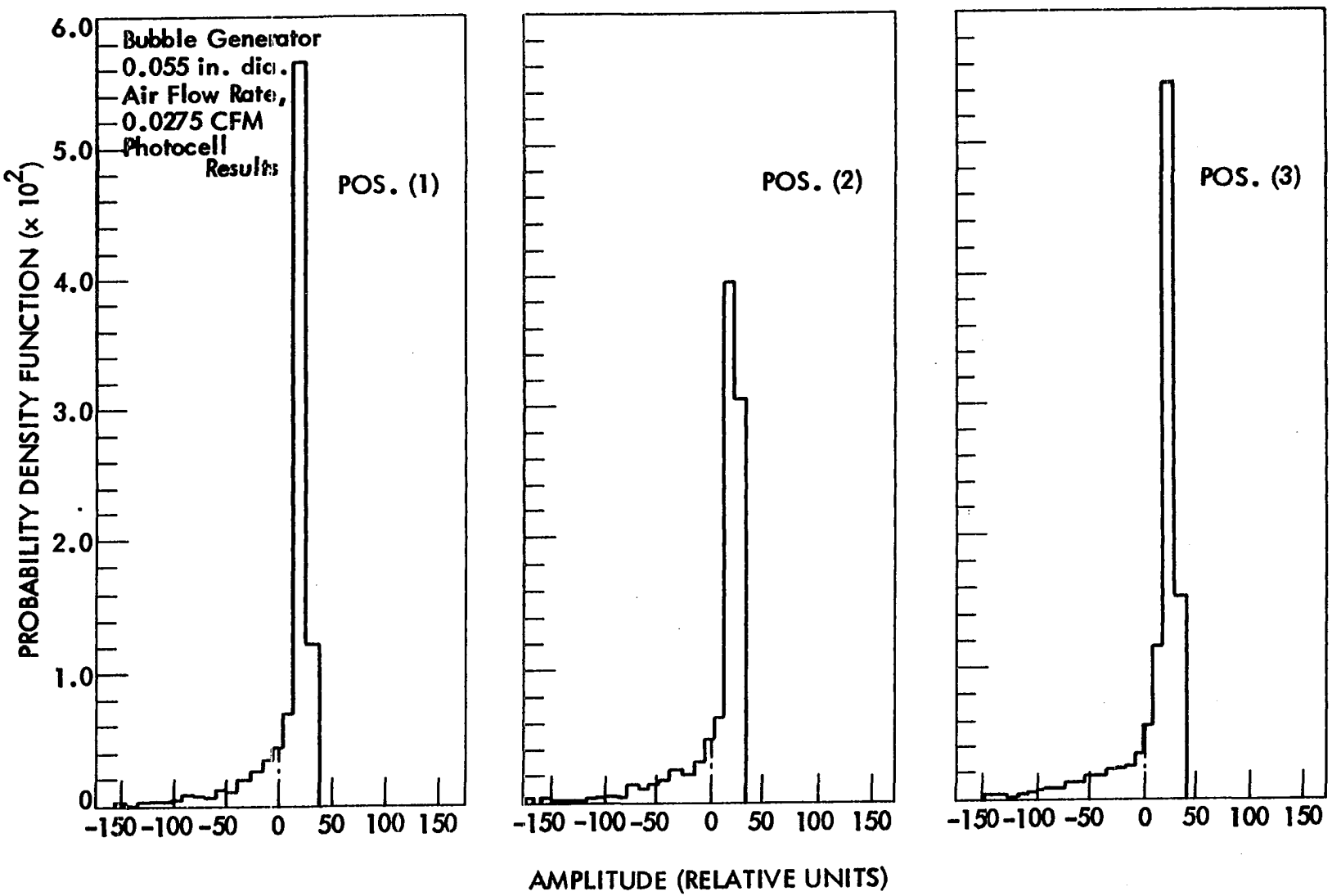

Fig. 25. Probability density function of air voids with a 0.055 in. dia. bubble generator and 0.0275 CFM air flow rate by photocell detector.

tor in Fig. 18, Fig. 25 shows the same trend of the response of noise signals due to void fluctuations.

2. Analytical results

To confirm the derived result given in Eq. (3.9) and the experimental and visual results obtained in this study, two noise signals, one a Gaussian noise with a magnitude of 1.5 RMS volts, the other a sinusoidal signals of 2 sin ($2\pi 30t$), were used to simulate time records of void fluctuations. The calculations of the PDF's were made by using Eq. (3.9). The right-hand side of Eq. (3.9) was multipled by minus one to match the polarity of the output of the experimental data from the picoammeter. Fig. 26 shows the PDF's of a Gaussian void fluctuation noise with different λ's. When λ increases, it implies that $|\lambda\alpha'(t)|$ increases. As shown in this figure, increasing λ increases the skewness of the detection process. The same trends of the shape change of the PDF's are also shown in the experimental results, for examples, Figs. 17 and 20. This confirms that Eq. (3.9) represents the response of the detector due to void fluctuations. As shown in Eq. (3.10), a linear relationship exists between the void fluctuation and the detection process only when $|\lambda\alpha'(t)|$ is very much less than one.

The PDF's of a sinusoidal void fluctuation signal with different λ's are shown in Fig. 27. The unsymmetric probability density functions of void fluctuations further indicate the nonlinear relationship between the detection process and void fluctuations. The similar shapes of the PDF's in Fig. 27, as compared with those of the experimental results, such as in Figs. 19 and 24, give a clue that some type of sinusoidal fluctuation func-

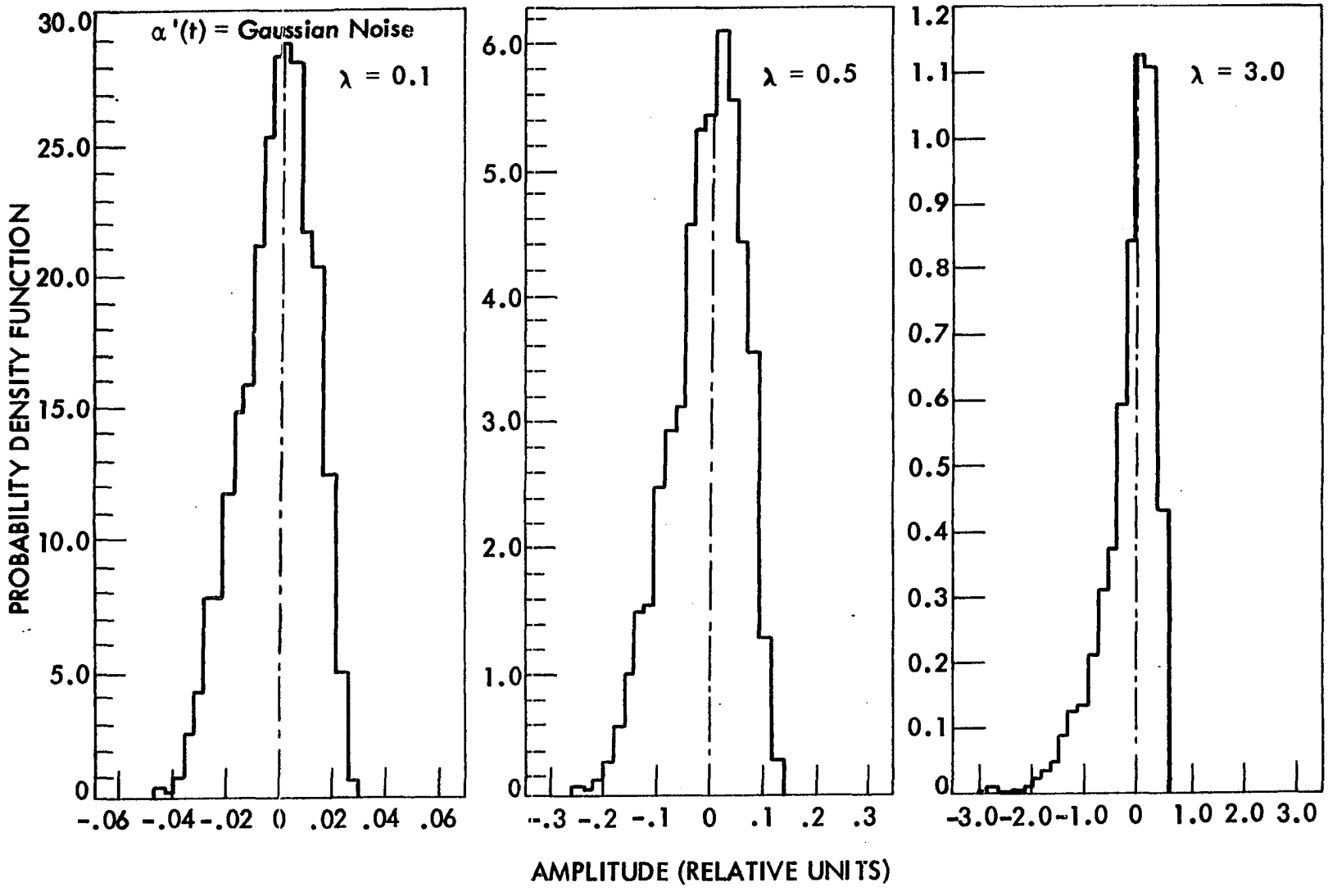

Fig. 26. Probability density function of a Gaussian void fluctuation with different λ's

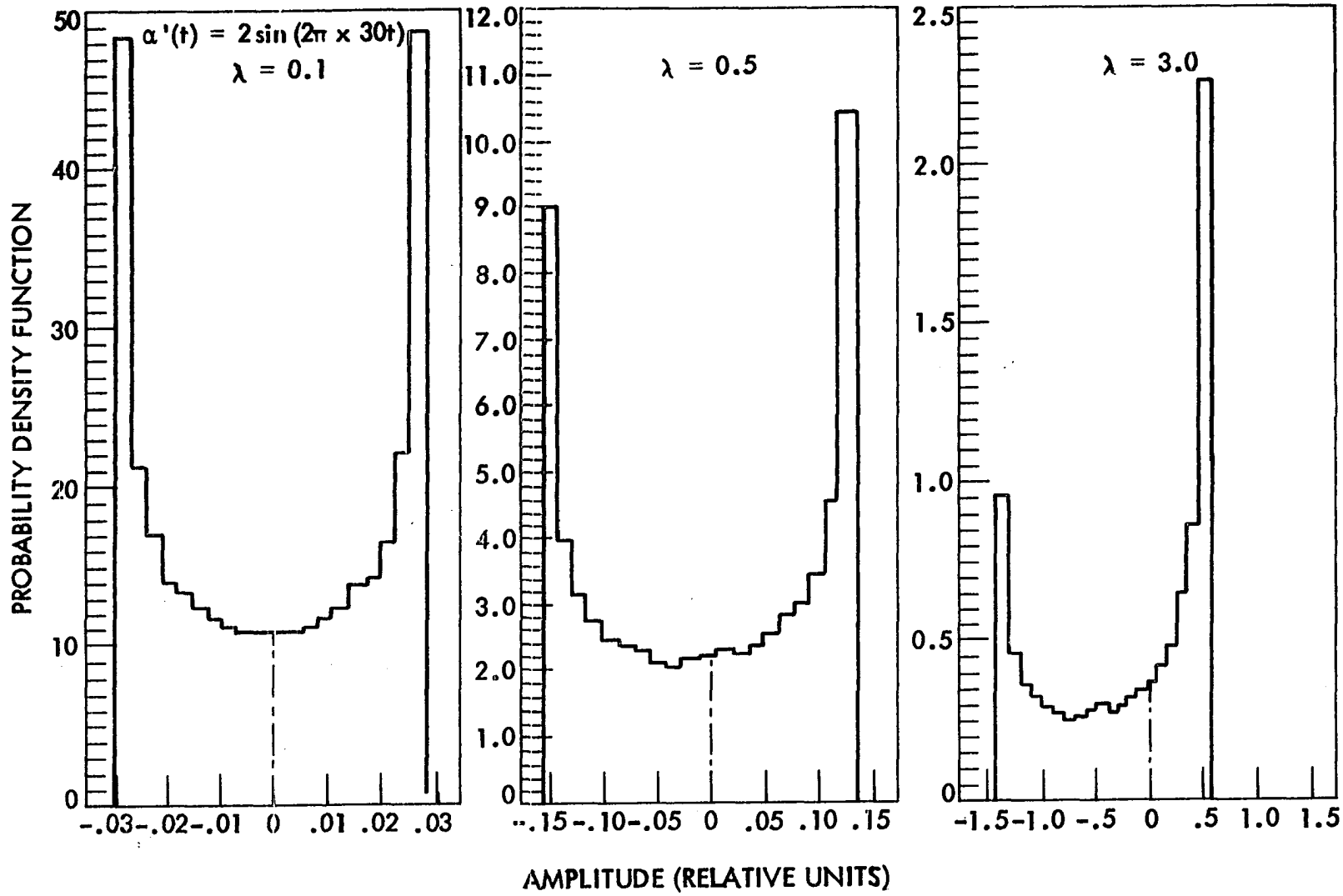

Fig. 27. Probability density function of a sinusoidal void fluctuation with different λ's

tion (or at least periodic) of the voids may exist in the coolant channel. This would be the case for slug flow, where alternate volumes of water and voids pass the detector.

C. Data of Auto-Power Spectral Densities

The auto-power spectral density (APSD) of noise signals provides information of void fluctuations in the frequency domain. This information is important in recognizing the characteristics of void fluctuations in terms of several parameters such as the bubble size and flow conditions in the channel.

Table 2 lists the APSD's of air void fluctuations based on changes of parameters during a series of data runs. Typical results of the APSD's are also shown in Figs. 28 through 32. Figure 28 shows the APSD of the air void fluctuations, as a function of detector position along the channel, for a 0.055-inch diameter bubble generator with an air flow rate of 0.004 CFM. In Figs. 29 and 30, the air flow rates were increased to 0.0275 CFM and 0.061 CFM, respectively, but with the same bubble generator size. These results illustrate that the detector is very sensitive to void fluctuations. The APSD with air voids is significantly larger than the APSD of the background noise. For the higher flow rate, as shown in Fig. 30, the APSD at position (1) with voids is at least two orders of magnitude greater than the background. It is also noted that as the detector is moved along the channel, the magnitude and shape of the APSD changes. In comparison with the results of Fig. 29, Fig. 31 shows the APSD of air void fluctuation with the same air flow rate but with a different bubble generator. In Fig. 32, using the same bubble generator as that for Fig. 31,

Table 2. The APSD's of air void fluctuations by neutron detector measurements

Run no.	Bubble generator size (in. dia.)	Air flow rate (CFM)	Detector position	APSD			
				Low peak		High peak	
				Freq. (Hz)	Amplitude (relative units)	Freq. (Hz)	Amplitude (relative units)
1	0.0135	0.0207	POS. (3)	0.58	0.96×10^{-5}	-	-
			POS. (2)	0.45	0.95×10^{-5}	1.50	6.00×10^{-5}
			POS. (1)	0.37	2.60×10^{4}	2.53	2.60×10^{5}
2	0.0260	0.004	POS. (3)	0.31	1.90×10^{-4}	-	-
			POS. (2)	0.31	1.50×10^{-4}	1.68	5.40×10^{-5}
			POS. (1)	0.31	1.08×10^{-4}	2.83	2.32×10^{-5}
			POS. (½)	0.31	0.80×10^{-4}	3.81	0.38×10^{-5}
3	0.0260	0.0275	POS. (3)	0.43	4.60×10^{-4}	1.25	1.30×10^{-3}
			POS. (2)	0.43	3.60×10^{-4}	1.65	0.48×10^{-3}
			POS. (1)	0.49	1.25×10^{-4}	3.00	0.29×10^{-3}
4	0.0260	0.061	POS. (3)	-	-	1.55	4.00×10^{-3}
			POS. (2)	-	-	2.50	2.80×10^{-3}
			POS. (1)	0.55	7.00×10^{-4}	4.30	1.55×10^{-3}
5	0.0260	0.0275 24" water head	POS. (2)	0.49	5.40×10^{-4}	2.20	5.40×10^{-4}
			POS. (1)	0.49	8.50×10^{-4}	3.30	1.70×10^{-4}
			POS. (½)	0.49	6.50×10^{-4}	6.80	0.56×10^{-4}
6	0.0260	0.061 24" water head	POS. (2)	0.88	7.00×10^{-4}	2.60	3.20×10^{-3}
			POS. (1)	0.88	6.20×10^{-4}	4.20	1.50×10^{-3}
			POS. (½)	0.76	5.20×10^{-4}	7.23	0.28×10^{-3}
7	0.0260	0.0275 14" water head	POS. (1)	0.55	5.84×10^{-4}	4.18	1.71×10^{-4}
			POS. (½)	0.49	7.68×10^{-4}	5.70	0.48×10^{-4}

Table 2. (Continued)

Run no.	Bubble generator size (in. dia.)	Air flow rate (CFM)	Detector position	APSD Low peak Freq. (Hz)	APSD Low peak Amplitude (relative units)	APSD High peak Freq. (Hz)	APSD High peak Amplitude (relative units)
8	0.0260	0.061	POS. (1)	0.88	8.23×10^{-4}	4.43	1.12×10^{-3}
		14" water	POS. (½)	0.76	7.0×10^{-4}	8.09	0.20×10^{-3}
9	0.055	0.004	POS. (3)	0.31	1.51×10^{-4}	1.31	7.63×10^{-5}
			POS. (2)	0.31	0.93×10^{-4}	1.43	3.55×10^{-5}
			POS. (1)	0.31	1.41×10^{-4}	2.47	1.05×10^{-5}
			POS. (½)	0.37	0.68×10^{-4}	6.93	0.77×10^{-5}
10	0.055	0.0275	POS. (3)	-	-	1.62	3.49×10^{-3}
			POS. (2)	0.49	5.0×10^{-4}	2.53	1.63×10^{-3}
			POS. (1)	0.49	3.5×10^{-4}	3.75	0.34×10^{-3}
			POS. (½)	0.49	4.16×10^{-4}	6.62	0.15×10^{-3}
11	0.055	0.061	POS. (3)	-	-	1.37	6.37×10^{-3}
			POS. (2)	0.82	7.0×10^{-4}	2.72	4.69×10^{-3}
			POS. (1)	0.82	7.17×10^{-4}	4.30	2.00×10^{-3}
			POS. (½)	0.76	4.56×10^{-4}	7.48	0.42×10^{-3}
12	0.1015	0.0207	POS. (3)	0.49	4.09×10^{-4}	1.61	3.50×10^{-3}
			POS. (2)	0.43	4.79×10^{-4}	2.22	1.62×10^{-3}
			POS. (1)	0.37	4.07×10^{-4}	3.94	0.23×10^{-3}
			POS. (½)	0.43	2.20×10^{-4}	7.11	0.09×10^{-3}
13	0.1015	0.0275	POS. (3)	0.31	6.00×10^{-4}	1.56	4.50×10^{-3}
			POS. (2)	0.43	6.40×10^{-4}	3.14	2.50×10^{-3}
			POS. (1)	0.49	5.12×10^{-4}	4.24	0.46×10^{-3}
			POS. (½)	0.49	2.73×10^{-4}	7.41	0.14×10^{-3}

Table 2. (Continued)

Run no.	Bubble generator size (in. dia.)	Air flow rate (CFM)	Detector position	APSD			
				Low peak		High peak	
				Freq. (Hz)	Amplitude (relative units)	Freq. (Hz)	Amplitude (relative units)
14	0.1015	0.061	POS. (3)	-	-	1.56	5.08×10^{-3}
			POS. (2)	-	-	2.41	4.36×10^{-3}
			POS. (1)	0.76	9.03×10^{-4}	3.63	1.92×10^{-3}
			POS. (½)	0.55	2.88×10^{-4}	7.20	0.59×10^{-3}
15	0.1015	0.004	POS. (3)	-	-	-	-
			POS. (2)	-	-	-	-
			POS. (1)	0.37	2.00×10^{-4}	3.51	1.05×10^{-4}
			POS. (½)	0.37	0.67×10^{-4}	3.69	0.64×10^{-4}

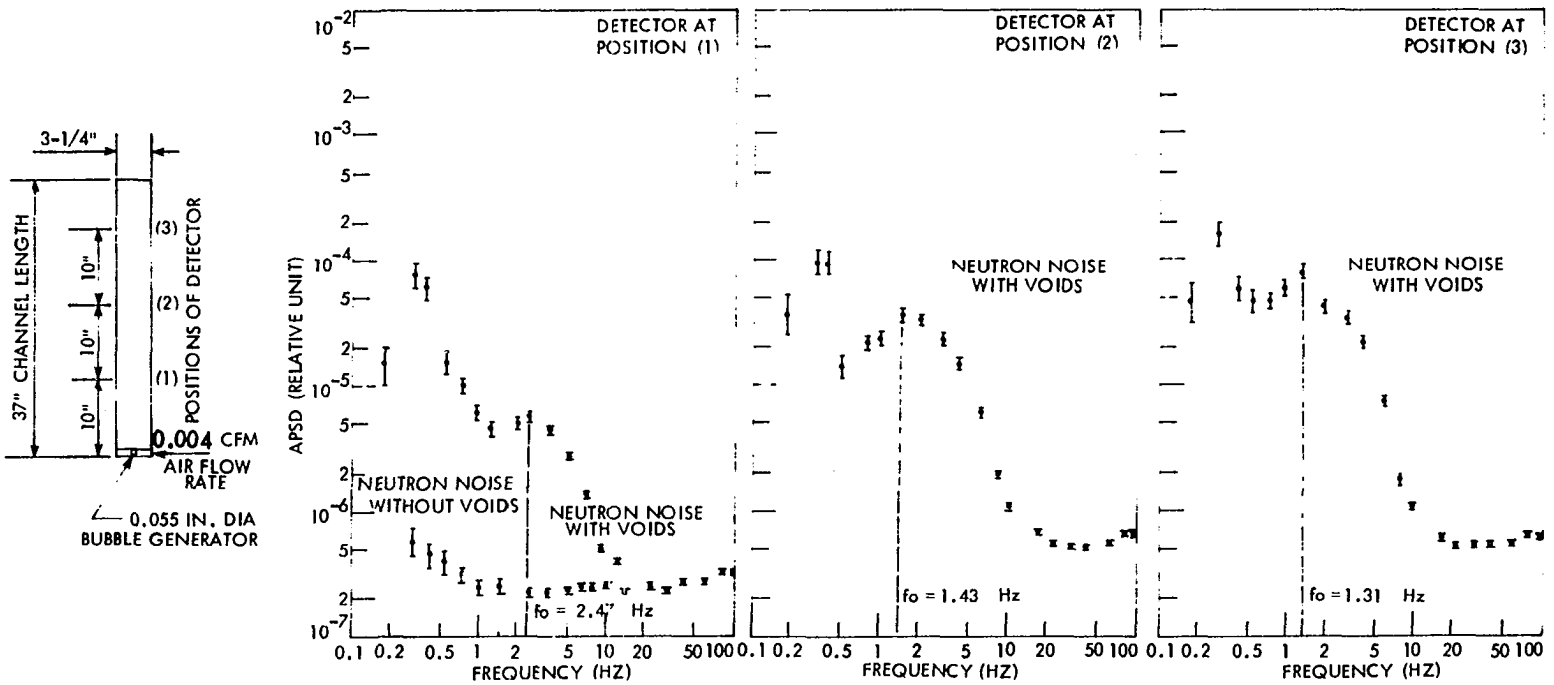

Fig. 28. Auto-power spectral density (APSD) of air voids with a 0.055 in. dia. bubble generator and 0.004 CFM air flow rate

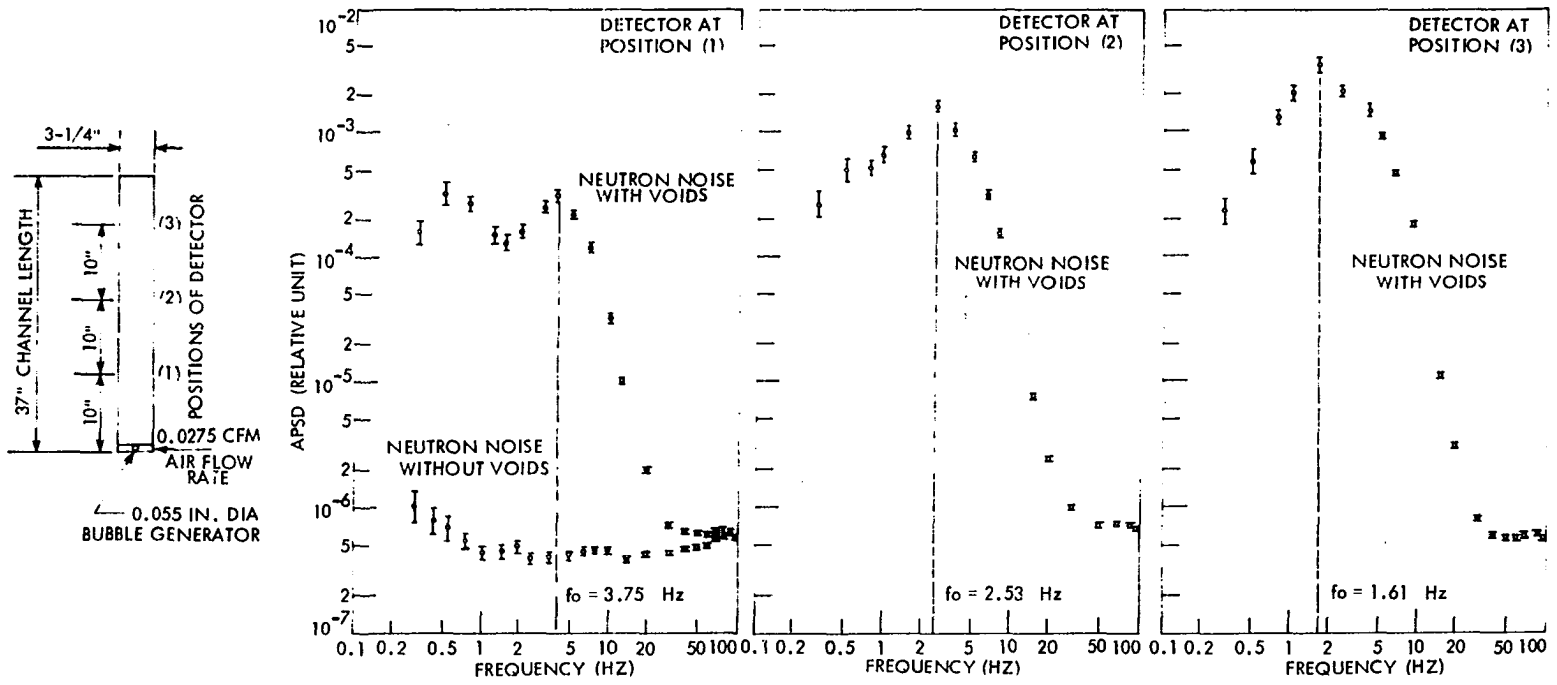

Fig. 29. Auto-power spectral density (APSD) of air voids with a 0.055 in. dia. bubble generator and 0.0275 CFM air flow rate.

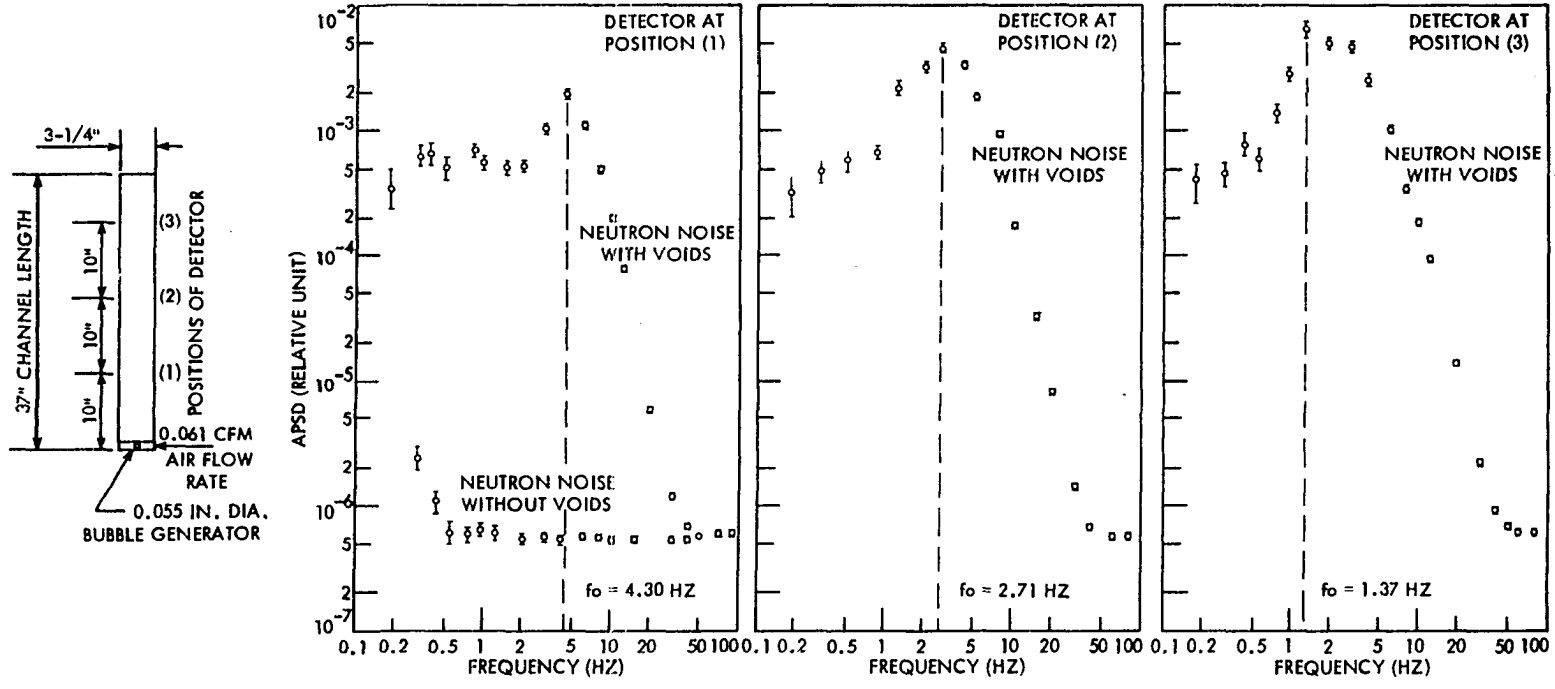

Fig. 30. Auto-power spectral density (APSD) of air voids with a 0.055 in. dia. bubble generator and 0.061 CFM air flow rate

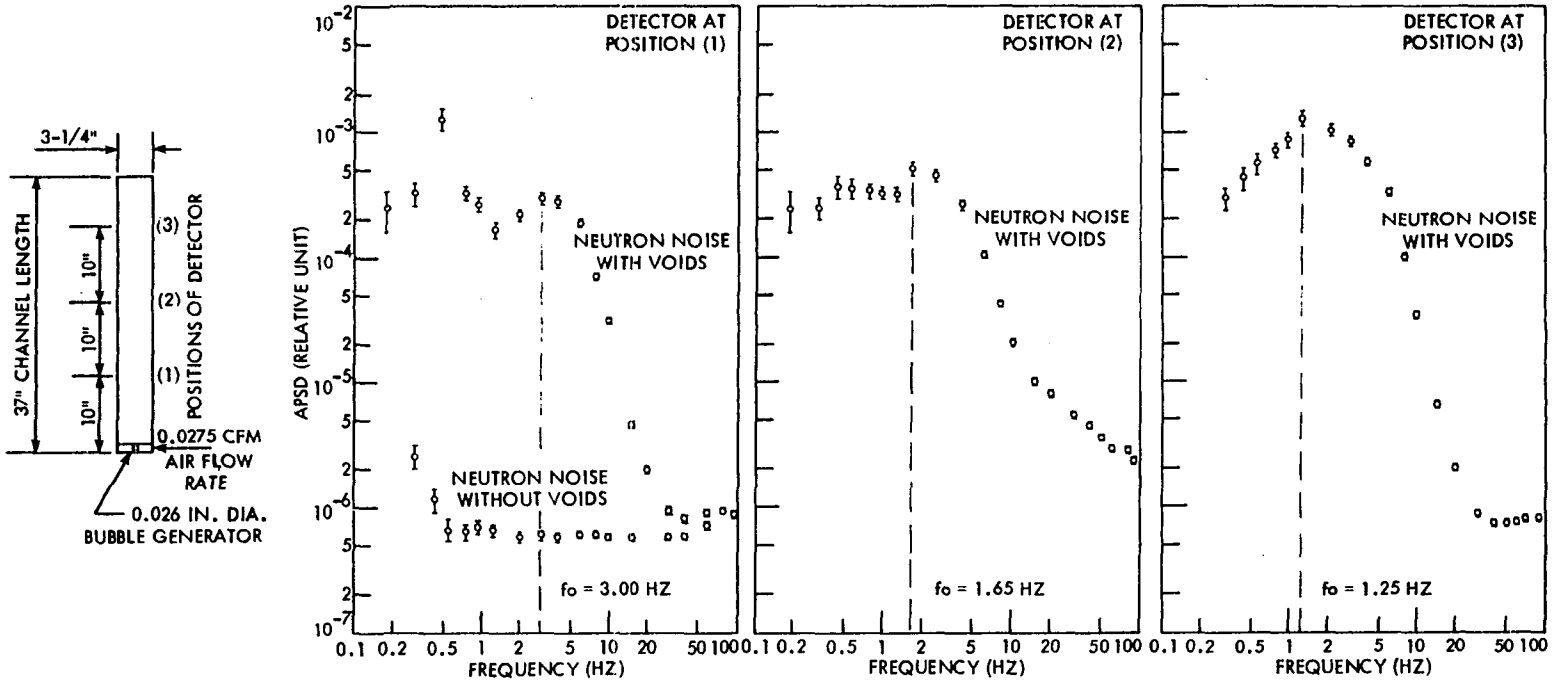

Fig. 31. Auto-power spectral density (APSD) of air voids with a 0.026 in. dia. bubble generator and 0.0275 CFM air flow rate

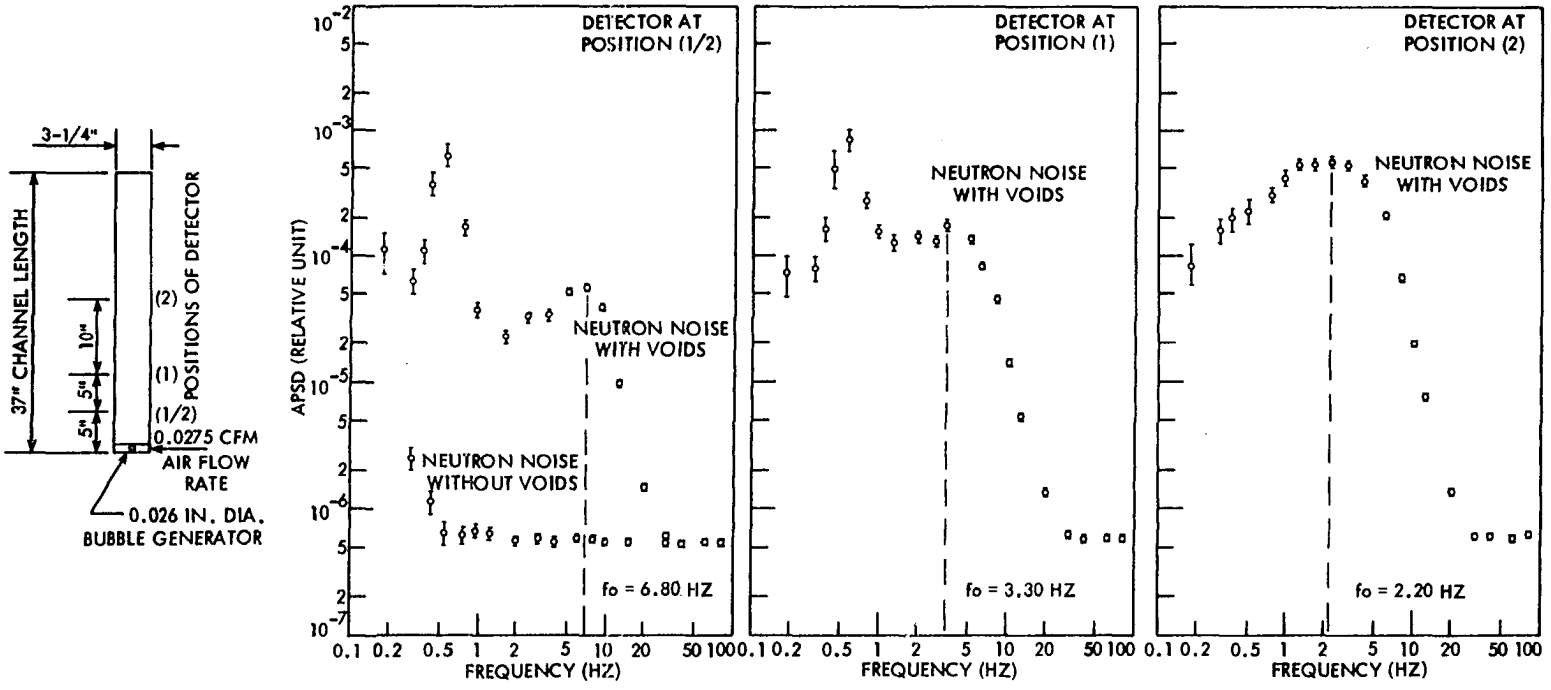

Fig. 32. Auto-power spectral density (APSD) of air voids with 24 in. water head, 0.026 in. dia. bubble generator and 0.0275 CFM air flow rate

the water head in the channel was reduced to 24 inches. The results indicate that the water head (or pressure) in the coolant channel is also one important factor affecting void fluctuations.

Two peaks are shown in most of the APSD results of Table 2 and the figures. The lower frequency peak is due to the helical motion of voids along the channel. This type of motion was observed and presented in Ref. 56. The higher peak in the spectrum at each position is believed due to the presence of partial slug flow in the channel [26,57]. The lower peak does not appear in some cases, for example at position (3) of Fig. 30. This is due to the dominating fluctuations of partial slug flow at that position.

The results of the APSD measurements, for steam voids at 80 watts, 180 watts, and 820 watts of heater power, are given in Table 3 and are also shown in Figs. 33, 34, and 35. The same general trends indicated in those figures of air void fluctuations are also apparent here.

Table 4 shows the APSD of air void fluctuations obtained by using the photocell detector measurements. Typical results of the APSD, corresponding to the PDF's obtained by the photocell detector in Fig. 25, are shown in Fig. 36. The similar responses of the photocell detector, compared to those of the neutron detector, help to confirm the measurements of void fluctuations in this study.

The APSD's of the background noise as shown in Figs. 28 through 35 indicate that a "nonwhite" spectrum exists at the lower frequencies. This is considered to be contributions from two components: (a) the transfer function of the nuclear reactor and (b) the presence of trends in the data,

Table 3. The APSD's of steam void fluctuations by neutron detector measurements

Run no.	Heater power (watts)	Detector position	APSD			
			Low peak		High peak	
			Freq. (Hz)	Amplitude (relative units)	Freq. (Hz)	Amplitude (relative units)
1	80	POS. (3)	0.82	3.04×10^{-4}	1.68	3.00×10^{-4}
		POS. (2)	0.76	3.93×10^{-4}	2.29	3.79×10^{-4}
		POS. (1)	0.55	0.44×10^{-4}	3.87	0.12×10^{-4}
2	180	POS. (3)	-	-	3.26	2.65×10^{-3}
		POS. (2)	0.55	5.50×10^{-4}	3.32	0.57×10^{-3}
		POS. (1)	0.49	1.50×10^{-4}	4.42	0.09×10^{-3}
3	320	POS. (3)	-	-	3.75	4.94×10^{-3}
		POS. (2)	-	-	4.06	3.72×10^{-3}
		POS. (1)	0.82	4.30×10^{-4}	6.00	0.25×10^{-3}

e.g. the d-c component. The latter component is particularly dominant in the background noise data from the photocell detector as shown in Fig. 36.

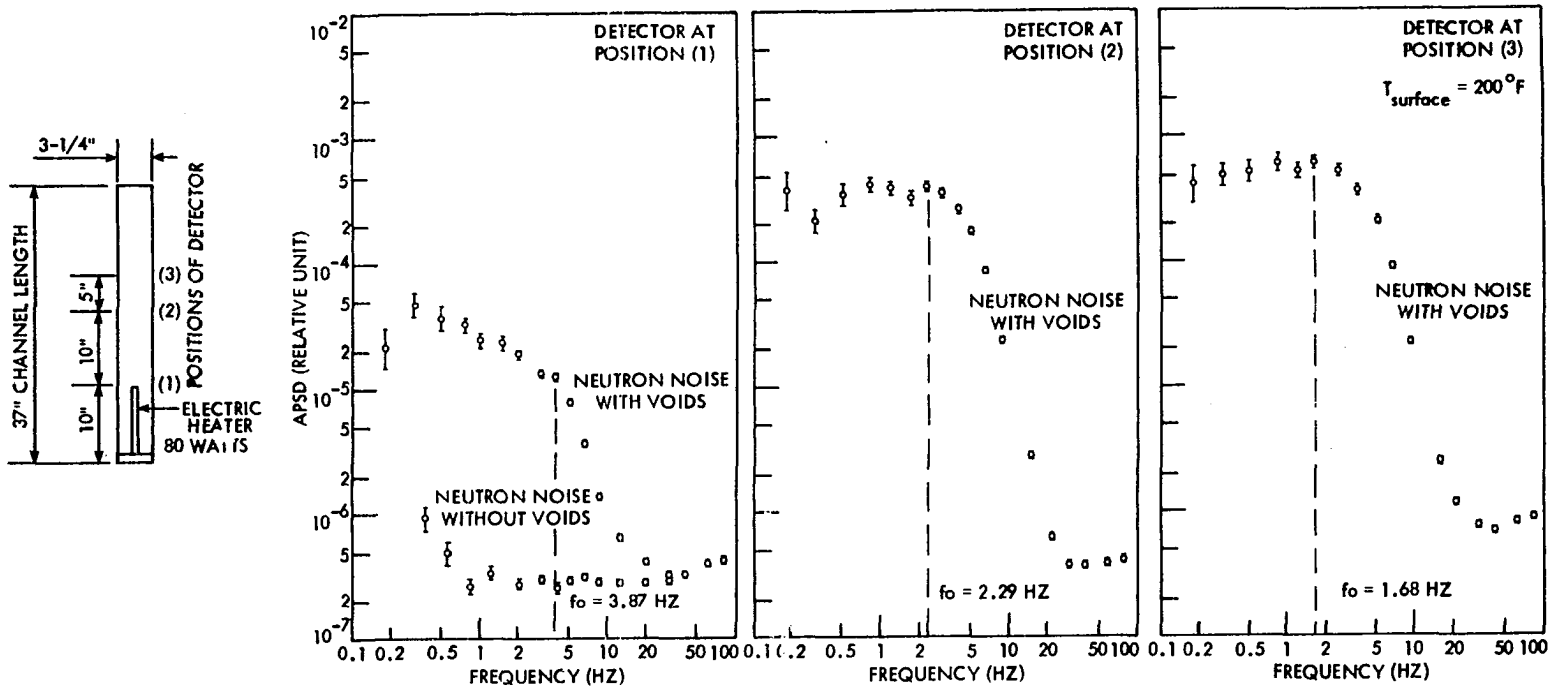

Fig. 33. Auto-power spectral density (APSD) of steam voids with 80 watts of heater power

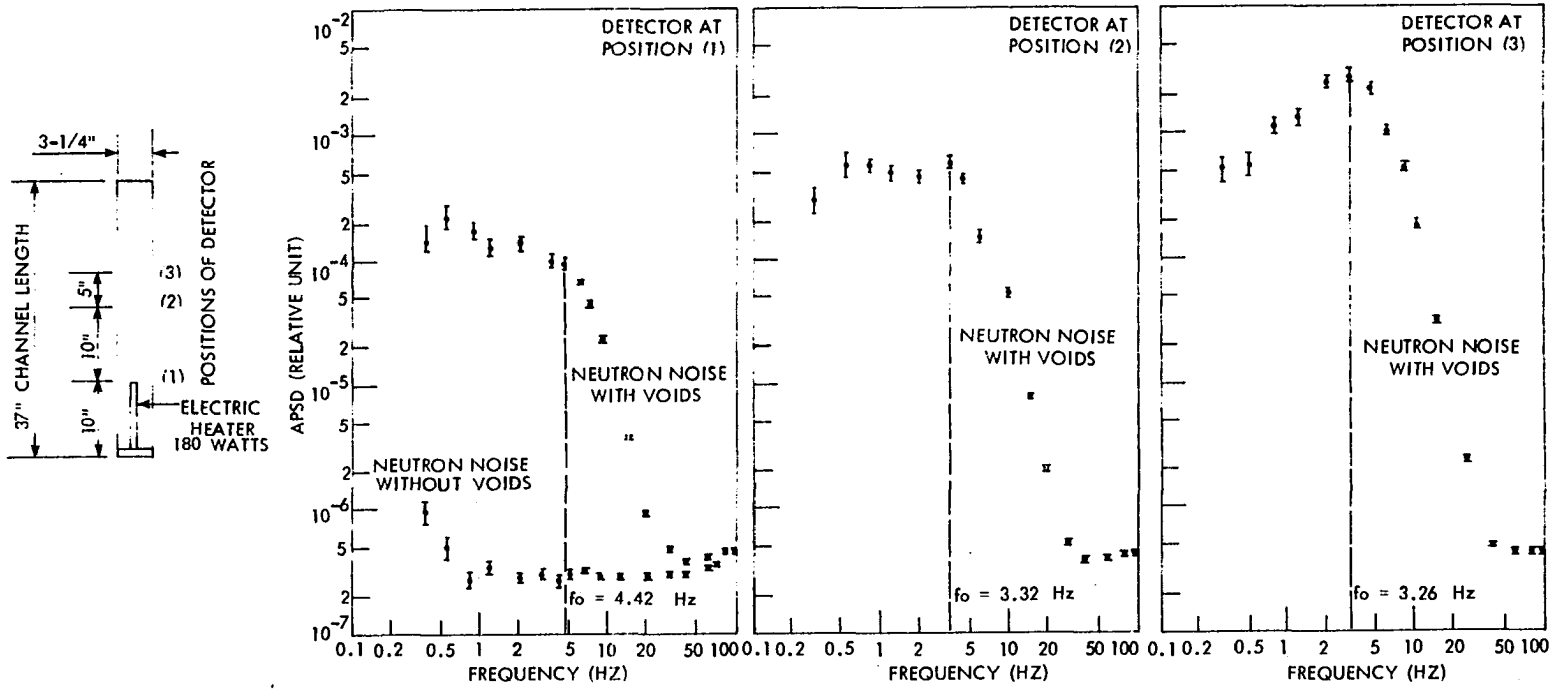

Fig. 34. Auto-power spectral density (APSD) of steam voids with 180 watts of heater power.

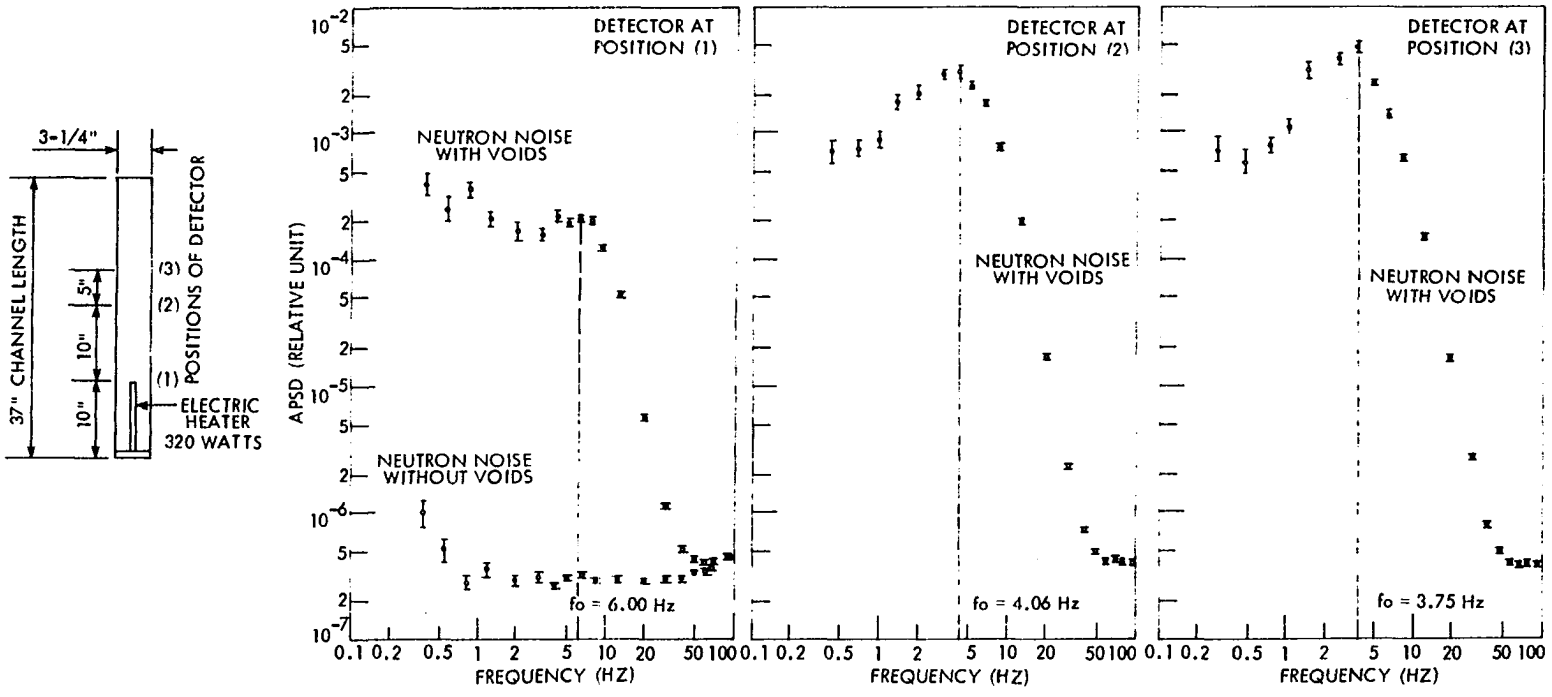

Fig. 35. Auto-power spectral density (APSD) of steam voids with 320 watts of heater power

Table 4. The APSD's of air void fluctuations by photocell detector measurements

Run no.	Bubble generator size (in. dia.)	Air flow rate (CFM)	Detector position	APSD			
				Low peak		High peak	
				Freq. (Hz)	Amplitude (relative units)	Freq. (Hz)	Amplitude (relative units)
1	0.026	0.0275	POS. (3)	0.37	6.5×10^{-6}	0.95	4.2×10^{-6}
			POS. (2)	0.49	4.4×10^{-6}	1.70	3.8×10^{-6}
			POS. (1)	0.37	5.4×10^{-5}	2.80	2.2×10^{-6}
			POS. (½)	0.37	2.0×10^{-6}	4.50	2.6×10^{-6}
2	0.026	0.0275 24" water head	POS. (2)	0.55	5.0×10^{-6}	1.49	4.0×10^{-6}
			POS. (1)	0.55	3.6×10^{-6}	3.50	2.4×10^{-6}
			POS. (½)	0.55	5.0×10^{-6}	3.20	2.6×10^{-6}
3	0.026	0.0275 14" water head	POS. (1)	0.55	5.6×10^{-5}	2.45	3.2×10^{-6}
			POS. (½)	0.37	1.8×10^{-6}	7.50	2.5×10^{-6}
4	0.055	0.0275	POS. (3)	0.55	4.0×10^{-6}	2.30	4.8×10^{-6}
			POS. (2)	0.55	4.8×10^{-6}	2.30	3.5×10^{-6}
			POS. (1)	0.55	7.0×10^{-6}	5.80	2.3×10^{-6}
			POS. (½)	0.49	5.1×10^{-6}	8.50	3.7×10^{-6}
5	0.1015	0.0275	POS. (3)	0.55	3.8×10^{-6}	1.30	5.0×10^{-6}
			POS. (2)	0.55	3.6×10^{-6}	2.40	4.5×10^{-6}
			POS. (1)	0.55	7.5×10^{-5}	5.50	3.0×10^{-6}
			POS. (½)	0.31	1.6×10^{-6}	8.20	4.4×10^{-6}

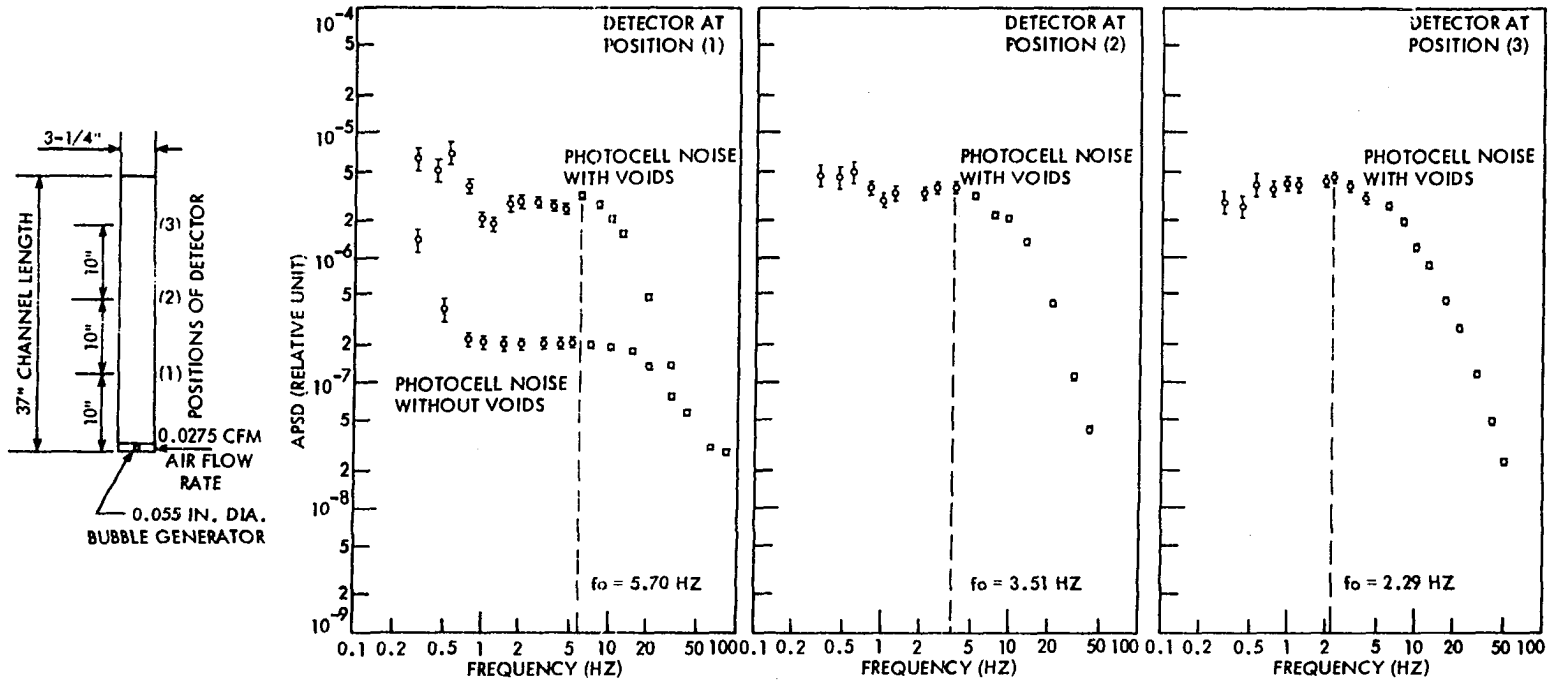

Fig. 36. Auto-power spectral density (APSD) of air voids with a 0.055 in. dia. bubble generator and 0.0275 CFM air flow rate by photocell detector

VII. DISCUSSION AND CONCLUSIONS

The general characteristics of the power spectral density functions and probability density functions of void fluctuations are consistent with the visual observations of void motion, the time-history records of void signals, and the characteristics of the equation derived in Chapter III.

Although the coolant channel and conditions used in this study differ from those in an actual nuclear power plant, the experiment based on the transmission of a thermal neutron beam through a water channel has shown that the detector is quite sensitive to the void fluctuations, and the response can be characterized in terms of the bubble size and flow conditions in the channel. The response of the detector due to void fluctuations in this experiment may be interpreted as the local noise source in the in-core detector in some cases. Such a condition could exist, for example, when an in-core detector is surrounded by a boiling medium with neutron diffusing from the adjacent fuel regions.

The present work can provide additional insights into the sources and significance of in-core detector noise when coolant boiling is taking place and lead to a better understanding of the local driving source. It also provides a basis for further work to develop a quantitative understanding of the parameters of voids which affect the local driving source of the in-core neutron detector.

Within the scope of the study, the following conclusions can be drawn:

(1) The detector response to void fluctuations observed by the transmission method of thermal neutrons is a nonlinear detection proc-

ess. The linear response only exists when the void fluctuations are very much small.

(2) The fluctuations of air voids in the coolant channel are comparable to those of steam voids.

(3) The void fluctuations are both time- and space-dependent.

(4) The void generation rate and size are the major factors in the void fluctuation characteristics.

(5) The power spectral density and probability density function are quite sensitive to the two-phase flow regime in the channel.

(6) The transmission of thermal neutrons through an open water channel that contains air or steam voids is well illustrated by the results of these measurements.

VIII. SUGGESTIONS FOR FUTURE WORK

Several suggestions for future research, which would lead to the ultimate goal of providing a quantitative understanding of void fluctuations in a coolant channel, are the following:

(1) A more realistic simulation of the local in-core detector noise can be made. Results of the simulation can be compared with those of this study.

(2) The effects of coolant circulation, heat source distributions, and system pressure can be studied for one or two detectors. The space-dependent effects of void fluctuations can be investigated by the two detector arrangement.

(3) The effects of void sizes, void size distributions, and void fractions in the coolant channel could be carried out.

(4) A detailed study of void thermalization effects in the coolant channel could aid in the interpretation of the results from an in-core detector.

(5) The two-phase flow regime in the coolant channel could be determined by using the results of noise analysis if parameters which affect the data of void fluctuations are well known.

IX. LITERATURE CITED

1. Harms, A, A., and C. F. Forrest. 1971. Dynamic effects in radiation diagnosis of fluctuating voids. Nucl. Sci. Engr. 46: 408-413.

2. Saxe, R. F. 1966. Detection of boiling in water-moderated nuclear reactors. Nucl. Safety 7: 452-456.

3. Nomura, T. 1968. Noise analysis of boiling water reactor. Pages 197-210 in Proceedings of the Japan-United States Seminar on Nuclear Reactor Noise Analysis, Tokyo and Kyoto, Japan.

4. Uhrig, R. E. 1973. State of the art of noise analysis in power reactors. CONF-730304 (ANS National Topical Meeting on Water Reactor Safety, Salt Lake City, Utah) 24 pp.

5. Thie, J. A. 1964. Noise sources in power reactors. Pages 357-368 in Proceedings of a Symposium on Noise Analysis in Nuclear Systems. University of Florida, Gainsville, Florida.

6. Stephenson, S. E., D. R. Roux, and D. N. Fry. 1966. Neutron fluctuation spectra in the Oak Ridge Research Reactor. ORNL-TM-1401 (Oak Ridge National Laboratory, Oak Ridge, Tennessee).

7. Saito, K. 1974. On the theory of power reactor noise-I, II, III. Annals Nucl. Sci. Engr. 1: 31-48, 107-128, 209-221.

8. Kosaly, G. 1973. Remarks on a few problems in the theory of power reactor noise. Nucl. Energy 14(3): 67-73.

9. Singh, O. P. 1974. On the reactor noise due to coolant flow fluctuations. Atomkernenergie 24: 65-66.

10. Seifritz, W. 1970. At-power reactor noise induced by fluctuations of the coooant flow. Atomkernerergie 16: 29-34.

11. Kosaly, G., and M. M. R. Williams. 1971. Point theory of the neutron noise induced by inlet temperature fluctuations and random mechanical vibrations. Atomkernenergie 18: 203-208.

12. Kosaly, G., and L. Nesko. 1972. Remarks on the transfer function relating inlet temperature fluctuations to neutron noise. Atomkernenergie 20: 33-36.

13. Lucia, A., E. Ohlmer, and D. Schwalm. 1973. Correlation between neutron noise and fuel element oscillations in the ECO-reactor. Atomkernenergie 22: 6-8.

14. Rajagopal, B. 1964. Reactor-noise measurements on Saxton reactor. Pages 427-447 in Proceedings of a Symposium on Noise Analysis in Nuclear Systems. University of Florida, Gainesville, Florida.

15. Stegemann, D., P. Gebureck, A. T. Nikulski, and W. Seifritz. 1973. Operating characteristics of a boiling water reactor deduced from in-core measurements. Pages 15-1-15-17 in T. W. Kerlin, ed. Power Plant Dynamics, Control and Testing an Applications Symposium. University of Tennessee, Knoxville, Tennessee.

16. Seifritz, W. 1972. An analysis of the space dependent neutron flux density fluctuations at the Lingen Boiling Water Reactor (KWL) by methods of stochastic process. Atomkernenergie 19: 271-279.

17. Rothman, G. P. 1973. Neutron noise in boiling reactors. Atomkernenergie 21: 113-118.

18. Wach, D., and G. Kosaly. 1974. Investigation of the joint effect of local and global driving source in incore-neutron noise measurements. Atomkernenergie 23: 244-250.

19. Hannaman, G. W., and R. A. Danofsky. 1975. In-core neutron detector response model based on basic principles. Transactions of the American Nuclear Society 21: 479.

20. Mogil'ner, A. I. 1971. Noise associated with inhomogeneities in the heat carrier of a reactor. Soviet Atomic Energy 30: 629-634.

21. Seifritz, W., and D. Stegemann. 1971. Reactor noise analysis. Atomic Energy Review 9: 129-176.

22. Rehsenow, W. M., ed. 1964. Developments in Heat Transfer. The M.I.T. Press, Cambridge, Mass.

23. Holman, J. P. 1972. Heat Transfer. McGraw-Hill Book Company, New York.

24. Leppert, G., and C. C. Pitts. 1964. Boiling. Adv. Heat Transfer 1: 185-266.

25. Tong, L. S. 1965. Boiling Heat Transfer and Two-Phase Flow. John Wiley & Sons, Inc., New York.

26. Wallis, G. B. 1969. One-Dimensional Two-Phase Flow. McGraw-Hill Book Company, New York.

27. Lahey, R. T., Jr. 1974. Two-phase flow in boiling water nuclear reactors. NEDO-13388 (General Electric Company, San Jose, Calif.).

28. El-Wakil, M. M. 1971. Nuclear Heat Transport. Intext Education Publishers, Scranton, Pa.

29. Houghton, G. 1961. Some theoretical aspects of vapor void formation in heated vertical channels. Nucl. Sci. Engr. 11: 121-128.

30. Houghton, G. 1962. An analysis of vapor profiles in heat channels. Nucl. Sci. Engr. 12: 390-397.

31. Levy, S. 1967. Forced convection subcooled boiling-prediction of vapor volumetric fraction. Inter. J. Heat and Mass Transfer 10: 951-965.

32. Sha, W. T. 1971. A generalized local boiling void model for light-water reactor system. Nucl. Sci. Engr. 44: 291-300.

33. Techy, Z., and L. Szabados. 1974. A theoretical basis of bubble motion in reactor channels. Atomkernenergie 23: 225-230.

34. Saxe, R. F. 1967. Survey of boiling detection methods in reactors. Pages 41-57 in Conference Proceedings of Incipient Failure Diagnosis for Assuring Safety and Availability of Nuclear Power Plants, Gatlinburg, Tennessee.

35. Saxe, R. F., W. H. Sides, and R. G. Foster, Jr. 1971. The detection of boiling in nuclear reactor. J. Nucl. Energy 25: 139-153.

36. Saxe, R. F. 1969. Considerations regarding the acoustical detection of boiling in the presence of cavitation. TID-25328 (Division of Technical Information, AEC, North Carolina State University).

37. Bonnet, J. A., Jr. and R. K. Osborn. 1971. Neutronic-acoustic detection of the onset of bulk boiling in liquid sodium. Nucl. Sci. Engr. 45: 314-320.

38. Boyd, L. R. 1959. Ion chamber can detect nucleate boiling. Nucleonics 17(3): 96-102.

39. De Shong, J. A., Jr. 1959. Flux, reactivity, steam void, and steam-water inter-layer noise spectrums in the EBWR. J. Nucl. Energy, Part A: Reactor Science 10: 147-156.

40. Colomb, A. L., and F. T. Binford. 1962. The detection of boiling in a water-cooled reactor, ORNL-TM-274 (Oak Ridge National Laboratory, Oak Ridge, Tennessee).

41. Thie, J. A. 1968. Noise in power reactors-a review of experiment, analysis, and theory. Reactor and Fuel-Processing Technology 11: 167-171.

42. Northern States Power Co. 1967. Pathfinder Atomic Power Plant Six Month Report. Northern States Power Co., Minneapolis, Minn.

43. Sha, W. T., and C. F. Bonilla. 1965. Out-of-pile steam-fraction determination by neutron-beam attenuation. Nucl. Appl. 1: 69-75.

44. Moss, R. A., and A. J. Kelly. 1970. Neutron radio-graphic study of limiting planar heat pipe performance. Intern. J. Heat Mass Transfer 13: 491-502.

45. Harms, A. A., S. Lo, and W. T. Hancox. 1971. Measurement of time-average voids by neutron diagnosis. J. Appl. Physics 42(10): 4080-4082.

46. Bendat, J. S., and A. G. Piersol. 1971. Random Data: Analysis and Measurement Procedures. John Wiley & Sons, Inc., New York.

47. Cooley, J. W., and J. W. Tukey. 1965. An algorithm for the machine calculation of complex Fourier series. Math. Computations 19: 144-154.

48. Davidson, J. F., and B. O. G. Schuler. 1960. Bubble formation at an orifice in a viscous liquid. Trans. Instn. Chem. Engrs. 38: 144-154.

49. Govier, G. W., B. A. Radford, and J. S. C. Dunn. 1957. The upwards vertical flow of air-water mixture, I. The Canadian J. Chem. Engr. 35: 58-70.

50. Govier, G. W., and W. L. Short. 1958. The upward vertical flow of air-water mixture, II. The Canadian J. Chem. Engr. 36: 195-202.

51. Brown, R. A. S., G. A. Sullivan, and G. W. Govier. 1960. The upward vertical flow of air-water mixture, III. The Canadian J. Chem. Engr. 38: 62-66.

52. Quandt, E. R. 1961. Analysis and measurement of flow oscillations. Pages 111-126 in the Fourth National Heat Transfer Conference, Buffalo, New York.

53. Wallis, G. B. 1961. Some hydrodynamic aspects of two-phase flow and boiling. Pages 319-340 in International Heat Transfer Conference, Boulder, Colorado.

54. Boure, J. A., A. E. Bergles, and L. S. Tong. 1973. Review of two-phase flow instability. Nucl. Engr. Design 25: 165-192.

55. Otnes, R. K., and L. Enochson. 1972. Digital Time Series Analysis. John Wiley & Sons, Inc., New York.

56. Miyagi, O. 1925. The motion of an air bubble rising in water. Phil. Mag. 50(295): 112-140.

57. Griffith, P., and G. B. Wallis. 1961. Two-phase slug flow. J. Heat Transfer 307-320.

X. ACKNOWLEDGMENTS

The author wishes to express special appreciation to his major professor, Dr. R. A. Danofsky, for his suggestions and encouragement in the pursuit of this study. The support of the Department of Chemical Engineering and Nuclear Engineering, and Engineering Research Institute for a research assistantship is acknowledged. In addition, the support of Ames Laboratory of the ERDA and the Engineering Research Institute for the experimental work is highly appreciated. The author is indebted to Mr. Michael Shewski for his help in accumulating the data. Finally, the author is deeply grateful to his wife, May-Hwai, for her help in typing the draft and for her understanding through the years of study.

XI. APPENDIX A:

CALCULATION OF AVERAGE VOID FRACTIONS FROM THE FLOW RATE

The average void fraction in the coolant channel is defined as

$$\bar{\alpha} = \frac{V_{bubble}}{V_{total}} \tag{A.1}$$

where

V_{bubble} = total volume of voids in the channel

and

V_{total} = total volume of liquid and voids in the channel.

In terms of volume rate in the channel, Eq. (A.1) can be expressed as

$$\bar{\alpha} = \frac{Qg}{Xo \cdot Z \cdot V_b} \tag{A.2}$$

$$= \frac{Qg}{A \cdot V_b} \tag{A.3}$$

where Qg = bubble flow rate in the channel

Xo = thickness of the coolant channel

Z = width of the coolant channel

V_b = average velocity of bubbles in the channel

A = cross-sectional area of the coolant channel.

The dimensions of the coolant channel are shown in Fig. A.1.

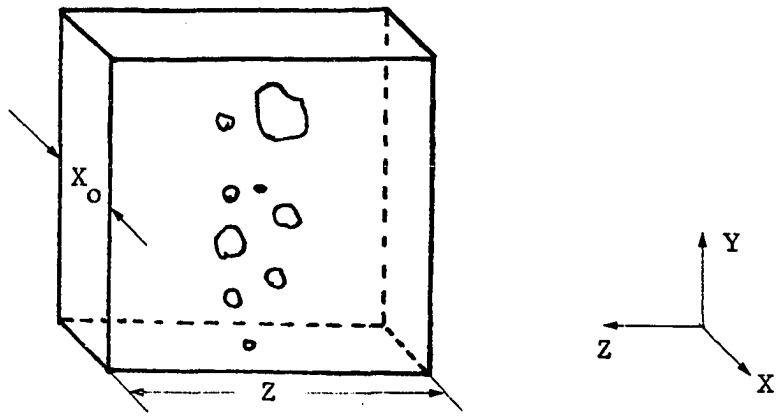

Fig. A.1. Dimensions of the channel

The air flow rate, Qg, is obtained from the reading of the flow rate meter. The cross-sectional area, A, is a known value of the coolant channel. To determine the average velocity of bubbles in the coolant channel, the empirical formulae in Ref. 26 were used. The average (terminal) velocity of air voids depends on the size of the bubble and is determined for different ranges of the Reynolds number, Reb. Table A.1 shows the range of applicability and the formulae of the terminal velocity of voids. The nomenclature of Table A.1 follows Ref. 26.

To find the range of applicability for determining the terminal velocity, an approximate value of V_b must be known to determine the Reynolds number. This is obtained by using Fig. 9.2 of Ref. 26.

After the terminal velocity, V_b, and the flow rate, Qg, are obtained, the average void fraction can be calculated according to Eq. (A.3). A simple program has been written based on Table A.1 and Eq. (A.3) for average void fraction calculation.

Table A.1. Terminal velocity of single bubbles in liquids [26]

	Terminal velocity	Range of applicability
Region 1	$V_b = \frac{2R_b^{2\,a}(\rho_f-\rho_g)g}{9\mu_f}$	$Reb^{b}<2$
Region 2	$V_b = 0.33g^{0.76}\left(\frac{\rho_f}{\mu_f}\right)^{0.52} R_b^{1.28}$	$2<Reb<4.02G_1^{-0.214\,c}$
Region 3	$V_b = 1.35\left(\frac{\sigma}{\rho_f R_b}\right)^{0.50}$	$4.02G_1^{-0.214}<Reb<3.10G_1^{-0.25}$ or $16.32G_1^{0.144}<G_2^{\,d}<5.75$
Region 4	$V_b = 1.53\left(\frac{g\sigma}{\rho_f}\right)^{0.25}$	$3.10G_1^{-0.25}<Reb$ $5.75<G_2$
Region 5	$V_b = (gR_b)^{0.5}$	$R_b \geq 2\left(\frac{\sigma}{g\rho_f}\right)^{0.5}$

[a] $R_b = \left(\frac{\sigma R_o}{g\rho_f}\right)^{1/3}$ if R_o = size of bubble generator ≤ 0.1336 cm

$= \left(\frac{3\sigma R_o}{2g\rho_f}\right)^{1/3}$ if $R_o > 0.1336$ cm

[b] $Reb = 2\rho_f V_b R_b/\mu_f$

[c] $G_1 = g\mu_f^{\,4}/\rho_f\sigma^3$

[d] $G_2 = gR_b^{\,4}V_b^{\,4}\rho_f^{\,3}/\sigma^3$

XII. APPENDIX B:

RESULTS OF THE AVERAGE VOID FRACTION

Based on Eq. (A.3), the average void fractions of air voids for a series of data runs are listed in Table B.1.

Table B.1. Average void fractions of air voids

Run no.	Bubble generator size (in. dia.)	Air flow rate (CFM)	Average void fraction ($\bar{\alpha}$,%)
1	0.0135	0.0207	1.83
2	0.0260	0.0040	0.49
3	0.0260	0.0275	3.37
4	0.0260	0.0610	7.50
5	0.0550	0.0040	0.44
6	0.0550	0.0275	3.05
7	0.0550	0.0610	6.79
8	0.1015	0.0207	2.55
9	0.1015	0.0275	3.38
10	0.1015	0.061	7.51
11	0.1015	0.004	0.49

XII. APPENDIX C:

THE PRBDT COMPUTER PROGRAM LISTING

```
//B265PRDB   JOB  A0118,LU
//STEP1  EXEC  PL1LFCG,PARM.GO=PRINT,REGION.GO=96K,TIME.GO=2
//PL1L.SYSIN  DD  *
  PRBDT:   PROC OPTIONS(MAIN);
  DCL DAPT FILE;
  DCL  ERROR CHAR(1) EXTERNAL;
  DCL  (A(4096,1),B(4096)) BINARY FLOAT;
  DCL  (NOVAR,NO,NV,J,NPLOT) BINARY FIXED;
  DCL  (UBO(3),FREQ(22),PCT(22),STATS(5)) BINARY FLOAT;
  DCL  (ASUM,ABAR) BINARY FLOAT;
  DCL  (PDF(22),SINT) BINARY FLOAT;
  DCL  (I,K,L,LL) BINARY FIXED;
  NO=4096;  NV=1;  NOVAR=1;
  GET DATA(NPLOT);  PUT DATA(NPLOT) SKIP(3);
  DO L=1 TO NPLOT;
  GET FILE  (DAPT) EDIT(B) (16(X(18),255 F(6,0),F(6,0)));
  ASUM=0.0;
  DO I=1 TO NO;
  ASUM=ASUM+B(I);  END;
  ABAR=ASUM/NO;
  DO K=1 TO NO;
  B(K)=B(K)-ABAR;  END;
  UBO(1)=1000.;  UBO(3)=1000.;
  UBO(2)=22.;
  DO J=1 TO NO;
  A(J,1)=B(J); END;
  CALL TAB1(A,B,NOVAR,UBO,FREQ,PCT,STATS,NO,NV,SINT);
  DO LL=1 TO 22;
  PDF(LL)=PCT(LL)/(100.*SINT); END;
  PUT DATA(SINT,FREQ,PCT,STATS,PDF) SKIP(3);
  END;
  CLOSE FILE (DAPT);
  TAB1:  PROCEDURE (A,S,NOVAR,UBO,FREQ,PCT,STATS,NO,NV,SINT);
  DCL  ERROR EXTERNAL CHAR(1);
  DCL  (I,INN,INTX,J,K,NO,NOVAR,KK) BINARY FIXED;
```

```
DCL  (A(4096,1),S(4096),UBO(3),FREQ(22),PCT(22),STATS(5),
SCNT,VMIN,VMAX,SINT,TEMP)  BINARY FLOAT;
ERROR='0';
IF NOVAR <=0 | NOVAR >NV THEN DO;
ERROR='6'; GO TO S50; END;
IF NV<=0 | NO <=0 THEN DO;
ERROR='1'; GO TO S50; END;
INN=UBO(2);
DO J=1 TO INN;
FREQ(J)=0.0; PCT(J)=0.0; END;
DO J=1 TO 5;
STATS(J)=0.0; END;
IF UBO(1) > UBO(3) | UBO(2) <= 2.0 THEN DO;
ERROR='2'; GO TO S50; END;
DO I=1 TO NO;
IF S(I) ¬=0.0 THEN DO;
KK=I; VMIN=A(I,NOVAR); VMAX=VMIN;
GO TO S10; END;
END;
ERROR='3'; GO TO S50;
S10:
DO I=KK TO NO;
IF S(I)¬=0.0 THEN DO;
IF A(I,NOVAR) <VMIN THEN VMIN=A(I,NOVAR);
IF A(I,NOVAR) > VMAX THEN VMAX=A(I,NOVAR);
END; END;
STATS(4)=VMIN;  STATS(5)=VMAX;
IF UBO(1)=UBO(3) THEN DO;
UBO(1)=VMIN;  UBO(3)=VMAX;  END;
SINT=(UBO(3)-UBO(1))/(UBO(2)-2);
SCNT=0.0;
DO I=KK TO NO;
IF S(I)¬=0.0 THEN DO;
SCNT=SCNT+1.0;
STATS(1)=STATS(1)+A(I,NOVAR);
```

```
   STATS(3)=STATS(3)+A(I,NOVAR)**2;
   TEMP=UBO(1)-SINT;
   INTX=INN-1;
   DO J=1 TO INTX;
   TEMP=TEMP+SINT;
   IF A(I,NOVAR) < TEMP THEN DO;
   K=J; GO TO S20; END;
   END;
   IF A(I,NOVAR) >= TEMP THEN DO;
   FREQ(INN)=FREQ(INN)+1.0; GO TO S30; END;
   S20:  FREQ(K)=FREQ(K)+1.0;   END;
   S30:  END;
   DO J=1 TO INN;
   PCT(J)=FREQ(J)*100.0/SCNT;  END;
   STATS(2)=STATS(1)/SCNT;
   IF SCNT=1.0  THEN DO;
   ERROR='4'; STATS(3)=0.0; GO TO S50;  END;
   ELSE DO;
   TEMP=STATS(3)-STATS(1)*STATS(1)/SCNT;
   IF TEMP <=0.0 THEN DO;
   ERROR='5';
   STATS(3)=0.0; GO TO S50; END;
   ELSE STATS(3)=SQRT(TEMP/(SCNT-1.0)); END;
   S50:  END TAB1;
  END PRBDT;
//GO.IN  DD  *
//GO.SYSIN  DD  *
```

XIV. APPENDIX D:

THE PSFFT COMPUTER PROGRAM LISTING

```
//B265PSFF   JOB  A0118,LU
//STEP1  EXEC  PL1LFCG,PARM.GO=PRINT,REGION.GO=176K,TIME.GO=8
//PL1L.SYSIN  DD  *
  PSFFT:   PROC OPTIONS(MAIN);
  DCL  DAPT FILE;
  DCL  ERROR CHAR(1) EXTERNAL;
  DCL  OPT CHAR(1);  DCL F(4096) BINARY FLOAT;
  DCL  (H,DELTA,PI)  BINARY FLOAT; DCL (ASUM,ABAR) BINARY FLOAT;
  DCL  (NPNT,M,NPND,L,NSET,J,NPLT) BINARY FIXED;
  DCL  (A(4096),PSD(4096),B(8192)) BINARY FLOAT;
  DCL  (TP,PSUM) BINARY FLOAT; DCL S(4096) BINARY FLOAT;
  DCL  (L1,L2,L3,L4,L5,L6,L7,L8) BINARY FIXED;
  DCL  (STD1,STD2,STD3,STD4,STD5,STD6,STD7,STD8) BINARY FLOAT;
  DCL  SCLF BINARY FLOAT; DCL CUTFF BINARY FLOAT;
  GET DATA(NPLT); PUT DATA(NPLT) SKIP(3);
  PLOT:  DO JP=1 TO NPLT;
  GET DATA(NPNT,H,NSET,SCLF,CUTFF);
  PUT DATA(NPNT,H,NSET,SCLF,CUTFF) SKIP(2);
  NPND=2*NPNT;
  M=LOG2(NPND);
  PI=3.141592653;
  DELTA=2*H/NPNT;
  TP=NPNT*H; /* TP IS THE LENGTH OF DATA RECORD  */
  /*  CALCULATE AND PRINT OUT THE STANDARD ERRORS FOR DIFFERENT L'S  */
  L1=0.1*CUTFF*TP;  STD1=1/(L1*NSET)**0.5;
  L2=0.08*CUTFF*TP;  STD2=1/(L2*NSET)**0.5;
  L3=0.05*CUTFF*TP;  STD3=1/(L3*NSET)**0.5;
  L4=0.02*CUTFF*TP;  STD4=1/(L4*NSET)**0.5;
  L5=0.01*CUTFF*TP;  STD5=1/(L5*NSET)**0.5;
  L6=0.005*CUTFF*TP;  STD6=1/(L6*NSET)**0.5;
  L7=0.002*CUTFF*TP;  STD7=1/(L7*NSET)**0.5;
  L8=0.001*CUTFF*TP;  STD8=1/(L8*NSET)**0.5;
  PUT DATA (L1,L2,L3,L4,L5,L6,L7,L8) SKIP(2);
  PUT DATA (STD1,STD2,STD3,STD4,STD5,STD6,STD7,STD8) SKIP(3);
  /* OPEN THE INPUT FILE AND MAKE SURE THE NUMBER OF DATA POINTS BE IN
```

```
POWER OF TWO */
J=0;
SET:  J=J+1;
GET FILE(DAPT) EDIT(A) (16(X(18),255 F(6,0),F(6,0)));
/* TAKE THE D-C COMPONENT OFF FROM THE DIGITIZED DATA */
ASUM=0.;
DO I=1 TO NPNT;
ASUM=ASUM+A(I); END;
ABAR=ASUM/NPNT;
DO K=1 TO NPNT;
A(K)=(A(K)-ABAR)/SCLF; END;
/* TAPERING THE INPUT DATA BEFORE FFT, THIS IS REQUIRED FOR PSD  */
/* THE COSINE TAPER IS APPLIED IN THIS PROGRAM */
TAP:  DO K=1 TO NPNT;
IF K< NPNT/10 | K> .9*NPNT THEN
A(K)=A(K)*(COS(5*PI*(K-NPNT/2)/NPNT))**2;
END TAP;  /* END OF COSINE TAPERING  */
/* REARRANGE THE DATA POINTS TO BE IN REAL AND IMAGINARY PART
 BY PAIRS IN NPNT ADJACENT STORAGE LOCATIONS  */
DO I=1 TO NPND BY 2;
B(I)=A((I+1)/2); END;
DO JO=2 TO NPND BY 2;
B(JO)=0.;  END;
/* SET OPT FOR CALLING FFT*/
OPT='1'; /* FOR COMPLEX FOURIER CALCULATION*/
CALL FFT(B,M,OPT);
IF ERROR ¬='0' THEN DO;
PUT LIST ('*** ERROR IN FFT ***') SKIP(1);
GO TO EXIT;  END;
/* TO OBTAIN THE RAW PSD, THE FOLLOWING CALCULATIONS ARE NEEDED  */
DO I=1 TO  NPNT  BY 2;
A(I)=(1/0.875)*DELTA*(B(I)**2+B(I+1)**2);  END;
/* THE TERM, (1/0.875), IS THE CORRECT SCALE FACTOR WHEN THE COSINE
TAPER IS APPLIED */
/* TO SOOTH THE PSD, A NEIGHBORING ESTIMATE METHOD IS USED  */
```

```
SMOTH: /*  TO SMOOTH THE LOCAL PSD  */
DO KK=1 TO (NPNT-2*L1+2) BY 2;
F(KK)=(KK+1)/(2*TP);
IF F(KK) >CUTFF  THEN L=L1;
ELSE IF F(KK)<=CUTFF & F(KK)>0.5*CUTFF THEN L=L2;
  ELSE IF F(KK)<=0.5*CUTFF & F(KK)>0.1*CUTFF THEN L=L3;
       ELSE IF F(KK)<=0.1*CUTFF & F(KK)>0.04*CUTFF THEN L=L4;
       ELSE IF F(KK)<=0.04*CUTFF & F(KK)>0.015*CUTFF THEN L=L5;
       ELSE IF F(KK)<=0.015*CUTFF & F(KK)>0.005*CUTFF THEN L=L6;
       ELSE IF F(KK)<=0.005*CUTFF & F(KK)>0.002*CUTFF THEN L=L7;
            ELSE L=L8;
SUM: /*  SUMMATION OF LOCAL PSD  */
PSUM=0.;
DO JJ=KK TO (KK+2*L-2)BY 2;
PSUM=PSUM+A(JJ); END ;
F(KK)=F(KK)+(L-1)/(2*TP);
B(KK)=PSUM/L; END SMOTH;
/* STORE THE FIRST SET OF PSD IF MORE THAN ONE SET OF
DATA POINTS ARE SUPPLIED ON TAPE  */
IF NSET=1 THEN GO TO CAPS;
ELSE IF J=1 THEN GO TO STGE;
    ELSE GO TO ADD;
STGE:
DO KS=1 TO   NPNT   BY 2;
S(KS)=B(KS); END STGE;
GO TO SET;
ADD: /* ADD THE PSD POINT BY POINT  */
DO KAV=1 TO   NPNT   BY 2;
B(KAV)=(B(KAV)+S(KAV));   END ADD;
IF J=NSET THEN GO TO CAPS;
ELSE GO TO STGE;
CAPS:/* CALCULATE THE AVERAGE PSD AND VALUES WITH
        STANDARD ERRORS */
DO KP=1 TO  (NPNT-2*L1+2)  BY 2;
PSD(KP)=B(KP)/NSET;
```

```
   IF F(KP)>1.04*CUTFF THEN DO; A(KP)=PSD(KP)*(1.-STD1);
                  B(KP)=PSD(KP)*(1.+STD1);  END;
   ELSE  IF F(KP)<=1.04*CUTFF & F(KP)>0.53*CUTFF THEN DO;
         A(KP)=PSD(KP)*(1.-STD2); B(KP)=PSD(KP)*(1.+STD2);  END;
   ELSE  IF F(KP)<=0.53*CUTFF & F(KP)>0.11*CUTFF THEN DO;
         A(KP)=PSD(KP)*(1.-STD3); B(KP)=PSD(KP)*(1.+STD3);  END;
   ELSE  IF F(KP)<=0.11*CUTFF & F(KP)>0.045*CUTFF THEN DO;
         A(KP)=PSD(KP)*(1.-STD4); B(KP)=PSD(KP)*(1.+STD4);  END;
   ELSE  IF F(KP)<=0.045*CUTFF & F(KP)>0.0175*CUTFF THEN DO;
         A(KP)=PSD(KP)*(1.-STD5); B(KP)=PSD(KP)*(1.+STD5);  END;
   ELSE  IF F(KP)<=0.0175*CUTFF & F(KP)>0.006*CUTFF THEN DO;
         A(KP)=PSD(KP)*(1.-STD6); B(KP)=PSD(KP)*(1.+STD6);  END;
   ELSE  IF F(KP)<=0.006*CUTFF & F(KP)>=0.0025*CUTFF THEN DO;
         A(KP)=PSD(KP)*(1.-STD7); B(KP)=PSD(KP)*(1.+STD7);  END;
   ELSE DO; A(KP)=PSD(KP)*(1.-STD8); B(KP)=PSD(KP)*(1.+STD8); END;
   END CAPS;
   /*  PRINT OUT THE AVERAGE PSD AND THE PSD WITH
       STANDARD ERRORS    */
   DO KP=1 TO 400 BY 2;
   PUT DATA (F(KP),PSD(KP),A(KP),B(KP)) SKIP(1); END;
   DO KP=401 TO 2000 BY 10;
   PUT DATA (F(KP),PSD(KP),A(KP),B(KP)) SKIP(1); END;
   DO KP=2001 TO (NPNT-2*L1+2) BY 40;
   PUT DATA (F(KP),PSD(KP),A(KP),B(KP)) SKIP(1); END;
   END PLOT;
   CLOSE FILE(DAPT);
   EXIT:
   END PSFFT;
//GO.IN  DD  *
//GO.SYSIN  DD  *
```